



An arbitrary-order Cell Method with block-diagonal mass-matrices for the time-dependent 2D Maxwell equations

Bernard Kapidani^a, Lorenzo Codecasa^{b,*}, Joachim Schöberl^c

^a Department of Mathematics, École Polytechnique Fédérale Lausanne, CH-1015 Lausanne, Switzerland

^b Dipartimento di Elettronica, Informatica e Bioingegneria, Politecnico di Milano, I-20133 Milano, Italy

^c Institute for Analysis and Scientific Computing, Technische Universität Wien, A-1040, Vienna, Austria



ARTICLE INFO

Article history:

Available online 8 February 2021

Keywords:

Maxwell equations
Cell Method
Discontinuous Galerkin
Dual grids
Covariant mapping
High-order finite elements

ABSTRACT

We introduce a new numerical method for the time-dependent Maxwell equations on unstructured meshes in two space dimensions. This relies on the introduction of a new mesh, which is the barycentric-dual cellular complex of the starting simplicial mesh, and on approximating two unknown fields with integral quantities on geometric entities of the two dual complexes. A careful choice of basis functions yields cheaply invertible block-diagonal system matrices for the discrete time-stepping scheme. The main novelty of the present contribution lies in incorporating arbitrary polynomial degree in the approximating functional spaces, defined through a new reference cell. The presented method, albeit a kind of Discontinuous Galerkin approach, requires neither the introduction of user-tuned penalty parameters for the tangential jump of the fields, nor numerical dissipation to achieve stability. In fact an exact electromagnetic energy conservation law for the semi-discrete scheme is proved and it is shown on several numerical tests that the resulting algorithm provides spurious-free solutions with the expected order of convergence.

© 2021 Elsevier Inc. All rights reserved.

1. Introduction

We are concerned in what follows with efficient numerical solutions for the Maxwell initial boundary value problem (MIBVP), whose solution is needed to accurately describe the behaviour of radio-frequency devices in industry, and to explain experimental findings in electromagnetic theory.

The first really successful discretisation of the initial boundary value problem for Maxwell's equations was introduced by Yee in [1]. The underlying algorithm in 3+1 dimensions of space and time, which is also known as Finite-Difference Time-Domain (FDTD, see [2,3]), has enjoyed durable success in both academic and industrial applications. Nevertheless, a plethora of other methods has subsequently also been proposed, analysed and tested to account for its various shortcomings: ineffectiveness in the case of material discontinuities which cannot be aligned with the Cartesian axes and limited $\mathcal{O}(h^2 + \Delta t^2)$ order of convergence, where h and Δt are the discrete steps in the spatial and temporal grids, respectively. Without any pretence of being exhaustive, we mention in this introductory section some families of approaches which try to mend these drawbacks.

There are approaches based on conforming finite elements spaces (see [4,5] and references therein), which work on unstructured space grids and present (tangentially continuous) piecewise-polynomials vector basis functions of arbitrary

* Corresponding author.

E-mail addresses: bernard.kapidani@epfl.ch (B. Kapidani), lorenzo.codecasa@polimi.it (L. Codecasa), joachim.schoeberl@tuwien.ac.at (J. Schöberl).

degree (starting from the ones introduced by Nedelev in [6]). Unfortunately these approaches lose the efficiency inherent in the Yee algorithm, since the system matrices¹ which need to be inverted at every time-step are banded but not (block-)diagonal. This latter amenable structure can be retrieved if mass-lumping techniques are employed (e.g. [7–10]), where basis functions are strongly tied to inexact numerical integration rules and need to be completely re-computed (or are simply unavailable) if the order of approximation needs to be increased. Later developments led instead to the adoption of Discontinuous Galerkin (DG) Finite Element Method (FEM) approaches, which ignore the conformity constraint on the basis functions and use orthonormal bases (which in principle lead to spectral convergence rates) compactly supported inside each finite element in the spatial discretisation of the domain. This choice, of course, destroys the geometry of the continuous Maxwell system, introducing spurious numerical solutions which do not converge to physical ones as the mesh size h tends to zero, and the presence of which can be easily detected by applying the same discretisation method to solving the Maxwell eigenvalue problem (MEP) instead of the MIBVP [11]. Counter-measures can be taken, in the form of penalization terms for the tangential jumps in the approximated solutions: for example, using up-wind fluxes (as in [12]) eliminates spurious solutions by introducing numerical energy dissipation in the scheme, which fact can become unacceptable when long-time behaviours of electromagnetic systems have to be studied. On the other hand, symmetric-interior-penalty (SIP) schemes (see [13–15]) preserve the hyperbolic nature of the system by introducing more unknowns which live on the skeleton of the mesh and do not approximate any physical quantity. Furthermore, a positive definite scalar penalty parameter, which must be tuned by the algorithm's user in accordance with h and the maximum polynomial degree in the chosen bases, must also be inserted in the formulation.

There is a third class of mutually related methods which mimic more closely Yee's original algorithm: the Finite Integration Technique of [16,17], which recasts the equations in integral form to apply the Yee algorithm to general staggered cuboidal elements but does not improve the accuracy of the original method otherwise (although we note that higher order versions of the method restricted to Cartesian-orthogonal grids do exist, e.g. [18]), the cell method (CM) of [19–23], which is also developed on two spatial grids in the more general setting of unstructured meshes, where a dual mesh is constructed from the primal mesh, either as its barycentric-dual (a procedure we will review in the present contribution) or as its circumcentric one. These methods can be theoretically studied in a wider framework (see also [24,25]) of approaches particularly fitting for Maxwell's equations (since they encode the so-called De Rham complex), in which differential operators are discretised using only topological information about the input mesh and all the metric information is instead encapsulated in the mass-matrix (which is in this context much rather seen as a discrete Hodge-star operator, e.g. [26–29]). The structure-preserving nature of these methods comes at the price of not being able to extend their convergence order to a steeper asymptotic than $\mathcal{O}(h)$, or $\mathcal{O}(h^2)$ at best if strict conditions on the mesh are imposed (although we note that for static problems some promising results have been achieved by showing the equivalence of the CM to lowest order mixed high order schemes in [30]). This elusive higher order approximation remains a much desired property, since, far from material discontinuities, solutions of the MIBVP are smooth and oscillatory.

In the present paper we are strongly rooted by this latter framework: we are inspired from the set of basis functions introduced by Codicosa and co-authors in [21,23], and more recently studied in [31], where an equivalence between their formulation and a peculiar DG one using two barycentric-dual unstructured meshes and piecewise-constant basis functions was proven by some of the present authors. Building on this result, we show how to extend the method to arbitrary degree in the local polynomial basis functions.

The paper proceeds further as follows: in Section 2 the Maxwell Initial Boundary Value Problem (MIBVP) is introduced, in Section 3 we recall barycentric-dual cellular complexes as a mean to discretize the spatial domain of our system and we introduce non-conforming functional spaces defined on these complexes, Section 4 introduces a new weak formulation involving the new spaces and a proof is given for the electromagnetic energy conservation property of the ensuing semi-discrete algorithm. Section 5 provides the fully discretised new algorithm and gives some insight on the connection between our new arbitrary-order scheme and known lowest order ones, as they present the same explicit splitting of topological and geometric operators. Section 6 provides numerical experiments to validate the correctness and performance of the proposed method: particular focus is devoted to showing the spectral correctness of the method. Finally, some general remarks, open questions, and directions for future work conclude the paper in Section 7.

2. The continuous problem

We focus in the present paper on the following simplified two dimensional system of first-order partial differential equations: The unknowns $\mathbf{E}(\mathbf{r}, t)$ and $H(\mathbf{r}, t)$ are the electric and magnetic field, respectively. Since we set the problem in the \mathbb{R}^2 ambient space, we denote only one of the two unknown fields in bold-face: even if the notation of three dimensional vector calculus is preserved, $\mathbf{E}(\mathbf{r}, t)$ and all other vector fields in the formulation are in fact to be understood as (polar) vector fields living in the Cartesian plane, i.e. $\mathbf{E}(\mathbf{r}, t) \cdot \hat{\mathbf{z}} = 0$. On the other hand $H(\mathbf{r}, t)$ is a scalar (the vector magnetic field is $H(\mathbf{r}, t)\hat{\mathbf{z}}$, aligned with the z-axis). In the applied jargon of microwave engineers this is the so-called *Transverse-Magnetic* (TM) field:

¹ usually the mass-matrices.

$$\underline{\mathbf{J}}(\mathbf{r}, t) + \underline{\varepsilon}(\mathbf{r}) \partial_t \mathbf{E}(\mathbf{r}, t) = \nabla H(\mathbf{r}, t) \times \hat{\mathbf{z}}, \quad \mathbf{r} \in \Omega, \quad (2.1)$$

$$\mu(\mathbf{r}) \partial_t H(\mathbf{r}, t) = -\nabla \times \mathbf{E}(\mathbf{r}, t) \cdot \hat{\mathbf{z}}, \quad \mathbf{r} \in \Omega, \quad (2.2)$$

to be satisfied for all times t and for all $\mathbf{r} = x\hat{\mathbf{x}} + y\hat{\mathbf{y}}$ in Ω , where we assume the spatial domain Ω to be a bounded polygon, with boundary denoted $\partial\Omega$. We harmlessly abuse the notation by somewhat incorporating three-dimensional calculus operations in our bidimensional domain: it is well-understood that

$$\nabla H(\mathbf{r}, t) \times \hat{\mathbf{z}} := (\partial_y H(\mathbf{r}, t), -\partial_x H(\mathbf{r}, t))^T,$$

$$\nabla \times \mathbf{E}(\mathbf{r}, t) \cdot \hat{\mathbf{z}} := \partial_x E_y(\mathbf{r}, t) - \partial_y E_x(\mathbf{r}, t),$$

where $\mathbf{E}(\mathbf{r}, t) := (E_x(\mathbf{r}, t), E_y(\mathbf{r}, t))^T$ maps Ω into \mathbb{R}^2 and $H(\mathbf{r}, t)$ maps Ω into \mathbb{R} . In general we allow non-homogeneous Dirichlet boundary conditions on either field, but for ease of presentation, we will focus in the following on the magnetic field boundary conditions alone, i.e. we set:

$$H(\mathbf{r}, t) = H_s(\mathbf{r}, t), \quad \mathbf{r} \in \partial\Omega, \quad (2.3)$$

with $H_s(\mathbf{r}, t) \in H^1(\partial\Omega)$. For boundaries of open sets, we will use in the following the quantities $\hat{\mathbf{n}}(\ell)$ and $\hat{\mathbf{t}}(\ell)$ which denote, respectively, the normal and tangent unit vectors on a directed curve for which ℓ is the arc-length parameter. With the assumption of the unit vectors lying in the Euclidean plane, it holds:

$$\hat{\mathbf{n}}(\ell) = \hat{\mathbf{t}}(\ell) \times \hat{\mathbf{z}}, \quad (2.4)$$

pointwise. To make the system solvable we assume initial conditions

$$\underline{\varepsilon} \mathbf{E}(\mathbf{r}, 0) = \mathbf{D}_0(\mathbf{r}), \quad \mathbf{r} \in \Omega, \quad (2.5)$$

$$\mu H(\mathbf{r}, 0) = B_0(\mathbf{r}), \quad \mathbf{r} \in \Omega, \quad (2.6)$$

for given functions $\mathbf{D}_0(\mathbf{r}) \in [L^2(\Omega)]^2$, $B_0(\mathbf{r}) \in L^2(\Omega)$. In fact, when looking for weak solutions of (2.1)–(2.2) the minimal regularity required for space derivatives of the solution pair is given by standard real Sobolev spaces: namely $H(\mathbf{r}, t) \in H^1(\Omega)$, while $\mathbf{E}(\mathbf{r}, t) \in \mathbf{H}^{curl}(\Omega)$, with:

$$H^1(\Omega) = \left\{ v \in L^2(\Omega) \text{ s.t. } \nabla v \in [L^2(\Omega)]^2 \right\},$$

$$\mathbf{H}^{curl}(\Omega) = \left\{ \mathbf{v} \in [L^2(\Omega)]^2 \text{ s.t. } \nabla \times \mathbf{v} \cdot \hat{\mathbf{z}} \in L^2(\Omega) \right\},$$

where the standard $L^2(\Omega)$ space of square-integrable functions was used and where all derivatives are now taken in the distributional sense.

The convective electric current $\mathbf{J}(\mathbf{r}, t) \in [L^2(\Omega)]^2$ is the source-term which, together with boundary and initial conditions, causes the dynamics of electromagnetic fields. Finally, $\underline{\varepsilon} = \varepsilon_0 \underline{\varepsilon}_r$, $\mu = \mu_0 \mu_r$ are the dielectric permittivity and magnetic permeability, respectively, with μ_0 and ε_0 being experimental constants and $c_0 = (\mu_0 \varepsilon_0)^{-\frac{1}{2}}$ being the speed of light (i.e. the wave-speed of electromagnetic radiation) in a vacuum. We make some mildly restrictive assumptions on the material parameters: we consider, in all what follows, time-invariant materials (for which generalization to general dispersive ones is, as for all numerical methods, more involved and will be the object of future studies). We further assume the material parameters to be symmetric positive-definite (s.p.d. 2×2 matrix in the case of $\underline{\varepsilon}$, a scalar for μ) with piecewise-smooth and point-wise bounded (in space) real coefficients.

The general space-time dependent solution of the MIBVP, for positive end-time $T < +\infty$, will then live in Bochner-type spaces for both the electric and magnetic fields. However, we will hereinafter mainly focus on approximation spaces for the space variable, since we will be discretising time with finite differences (as in the Yee algorithm).

3. Barycentric-dual complexes and related broken spaces

We assume a regular partition of Ω into triangles to be available, which can be easily provided from any black-box mesher (e.g. [32,33]). Rigorously speaking, said partition is a simplicial complex. We define a simplicial complex for Ω , denoted \mathcal{C}^Ω , as a sequence of sets of simplexes of dimension going from zero to d (the ambient space). A simplicial complex is itself a particular kind of *cellular* (or *cell*) complex, which is the more general structure one gets by relaxing the requirement on geometric entities of \mathcal{C}^Ω from being simplexes to, for example, being generic polytopes (called k -cells instead of k -simplexes). Our starting mesh, as any given simplicial complex, possesses a dual complex, which we denote with $\tilde{\mathcal{C}}^\Omega$ and which is indeed a cellular complex *but not a simplicial one*. The existence of a dual cellular complex hinges on a sequence of one-to-one correspondences between k -simplexes in \mathcal{C}^Ω and $(d-k)$ -cells in $\tilde{\mathcal{C}}^\Omega$.

The geometric realization of such a dual cellular complex is non-unique. Yet, for what follows, it is a fundamental choice to construct $\tilde{\mathcal{C}}^\Omega$ as the barycentric-dual (see [19,20]) of \mathcal{C}^Ω : each vertex of the dual complex is the centroid of some

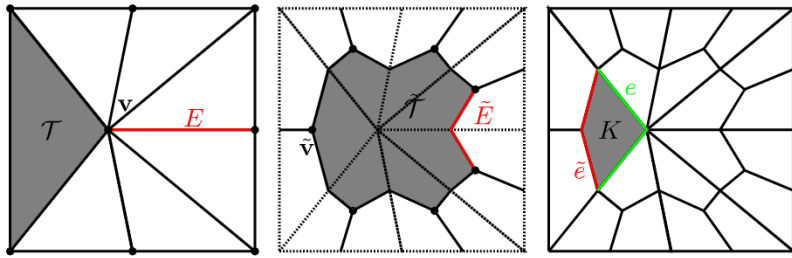


Fig. 1. The primal and dual complex: a glossary. On the left we mesh the unit square $\Omega = (0, 1) \times (0, 1)$ with the simplicial complex C^Ω and we show a vertex v , an edge E , and a triangle $T \in C^\Omega$. In the middle, where the primal complex is shown dashed, we have constructed the barycentric-dual complex: \tilde{v} is the dual to T , \tilde{E} is dual to E , and $\tilde{T} \in \tilde{C}^\Omega$ is dual to v . On the right, we finally draw the resulting auxiliary complex K^Ω and also emphasize a quadrilateral $K \in K^\Omega$, and edges e, \tilde{e} in its boundary, which comprises intersections with the skeletons of both primal and dual meshes.

triangle $T \in C^\Omega$, each dual edge of \tilde{C}^Ω is obtained as a poly-line joining the centroid of some edge in the starting mesh to the centroids of neighbouring triangles. Finally each dual cell $\tilde{T} \in \tilde{C}^\Omega$ is a (generally non-convex) polygon bounded by dual edges and is in one-to-one correspondence with a vertex of the primal mesh C^Ω . A depiction of one simplicial complex and its barycentric-dual companion is given in the two first leftmost panels of Fig. 1.

We will also need, for what lies ahead in the paper, to define an additional partition of the domain

$$\mathcal{K}^\Omega := \left\{ K = T \cap \tilde{T} \text{ s.t. } T \in C^\Omega, \tilde{T} \in \tilde{C}^\Omega, K \neq \emptyset \right\},$$

where we note that each d -dimensional simplex of the original mesh (and hence the whole of Ω) is thus further partitioned into $d+1$ disjoint subsets $K \in \mathcal{K}^\Omega$ (see again Fig. 1, rightmost panel). For any original triangle, we get three irregular quadrilaterals, which will be of utmost importance, and we will call *fundamental d -cells* (see the definition of *micro-cell* in [20] or see [31]) and denote with K in the rest of the paper. Having constructed the appropriate dual complex we can refer hereinafter to the starting simplicial one as the primal complex. We mention in passing the circumcentric-dual (see [19]) as another popular construction employed in the literature, which has amenable properties for finite volumes schemes (see [34] and references therein), but requires the triangulation of Ω to be a Delaunay one, which is often too restrictive and usually not satisfied by the meshing algorithm at hand.

We define, with reference to the barycentric-dual meshes introduced above, the *broken Sobolev spaces*

$$\mathbf{H}_{pw}^{curl}(\tilde{C}^\Omega) = \left\{ \mathbf{v} \in [\mathbf{L}^2(\Omega)]^2 \text{ s.t. } \mathbf{v}|_{\tilde{T}} \in \mathbf{H}^{curl}(\tilde{T}), \forall \tilde{T} \in \tilde{C}^\Omega \right\}, \quad (3.1)$$

$$\mathbf{H}_{pw}^1(C^\Omega) = \left\{ u \in \mathbf{L}^2(\Omega) \text{ s.t. } u|_T \in \mathbf{H}^1(T), \forall T \in C^\Omega \right\}, \quad (3.2)$$

where we have kept track of the fact that one of the two spaces is vector-valued. Informally speaking, these are locally conforming spaces which are globally non-conforming on Ω , yet the non-conformity has a different support for the two spaces.

In non-conforming DG methods, once a mesh is available, the equations are independently tested on each triangle against some polynomial basis (or some other kind of locally smooth functions, if the DG-FEM is combined with spectral or Trefftz approaches, e.g. [35]). This provides, once the solution is approximated within the same finite-dimensional basis, block-diagonal (hence easily invertible) mass-matrices on the left-hand side (l.h.s.) of the weak formulation of (2.1)–(2.2). We can here generate a similar block-diagonal structure by virtue of two newly defined broken spaces. To achieve this, our first step is to apply *local* testing in space to equations (2.1) and (2.2) with respect to the new broken spaces. Herein lies the main novelty of the present work as we exploit the two dual complexes by making the r.h.s. of the system ultra-weak. By performing a formal integration by parts, we introduce the following weak formulation of the problem (2.1)–(2.2):

$$\sum_{T \in C^\Omega} \int_{\tilde{T}} \mathbf{v} \cdot (\underline{\underline{\varepsilon}} \partial_t \mathbf{E} + \mathbf{J}) \, d\mathbf{r} = \sum_{\tilde{T} \in \tilde{C}^\Omega} \left(- \int_{\partial \tilde{T} \setminus \partial \Omega} \mathbf{v} \cdot H\hat{\mathbf{t}}(\ell) \, d\ell - \int_{\partial \tilde{T} \cap \partial \Omega} \mathbf{v} \cdot H_s \hat{\mathbf{t}}(\ell) \, d\ell + \int_{\tilde{T}} \nabla \times \mathbf{v} \cdot H\hat{\mathbf{z}} \, d\mathbf{r} \right), \quad (3.3)$$

$$\sum_{T \in C^\Omega} \int_T u (\mu \partial_t H) \, d\mathbf{r} = - \sum_{\tilde{T} \in \tilde{C}^\Omega} \left(\int_{\partial \tilde{T}} u \mathbf{E} \cdot \hat{\mathbf{t}}(\ell) \, d\ell - \int_{\tilde{T}} \hat{\mathbf{z}} \times \nabla u \cdot \mathbf{E} \, d\mathbf{r} \right), \quad (3.4)$$

$\forall \mathbf{v} \in \mathbf{H}_{pw}^{curl}(\tilde{C}^\Omega)$, and $\forall u \in \mathbf{H}_{pw}^1(C^\Omega)$, respectively. We stress the two different choices of local integration domains in the two weak equations and we note that boundary terms arise from the tangential discontinuity of test-functions. It is easy to check that the conventional weak curl would emerge if the appropriate conforming space were used. Naturally, the final system of equations must be stated in a finite-dimensional setting. To achieve this the finite dimensional subset of the

continuous spaces will be as usual piecewise polynomial (vectors) up to some fixed degree $p \geq 0$. Namely, we define the spaces:

$$\tilde{\mathbf{W}}^p = \mathbf{H}_{pw}^{curl}(\tilde{\mathcal{C}}^\Omega) \cap \mathbf{P}^p(\mathcal{K}^\Omega; \mathbb{R}^2), \quad \mathbf{W}^p = \mathbf{H}_{pw}^1(\mathcal{C}^\Omega) \cap \mathbf{P}^p(\mathcal{K}^\Omega; \mathbb{R}),$$

where $\mathbf{P}^p(\mathcal{K}^\Omega; \mathbb{R})$ is the space of piece-wise polynomials of degree at most p on each $K \in \mathcal{K}^\Omega$. We thus have that the two discrete spaces, although locally conforming on two different meshes, comprise of functions which are locally smooth on the same geometric object K . By choosing $\tilde{\mathbf{W}}^p$ and \mathbf{W}^p also as trial spaces for the approximation of the two unknown fields, we build up a new Galerkin formulation.

4. The new Galerkin formulation

Discretising space and keeping time continuous, we seek the solution pair $(\mathbf{E}^{h,p}(\mathbf{r}, t), H^{h,p}(\mathbf{r}, t)) \in [\mathbf{L}^2((0, T); \tilde{\mathbf{W}}^p)] \times [\mathbf{L}^2((0, T); \mathbf{W}^p)]$ such that

$$\sum_{\tilde{\mathcal{T}} \in \tilde{\mathcal{C}}^\Omega} \int_{\tilde{\mathcal{T}}} \mathbf{v} \cdot (\underline{\underline{\varepsilon}} \partial_t \mathbf{E}^{h,p} + \mathbf{J}) \, d\mathbf{r} = \sum_{\tilde{\mathcal{T}} \in \tilde{\mathcal{C}}^\Omega} \left(- \int_{\partial \tilde{\mathcal{T}} \setminus \partial \Omega} \mathbf{v} \cdot H^{h,p} \hat{\mathbf{t}}(\ell) \, d\ell - \int_{\partial \tilde{\mathcal{T}} \cap \partial \Omega} \mathbf{v} \cdot H_s \hat{\mathbf{t}}(\ell) \, d\ell + \int_{\tilde{\mathcal{T}}} \nabla \times \mathbf{v} \cdot H^{h,p} \hat{\mathbf{z}} \, d\mathbf{r} \right), \quad (4.1)$$

$$\sum_{\mathcal{T} \in \mathcal{C}^\Omega} \int_{\mathcal{T}} u (\mu \partial_t H^{h,p}) \, d\mathbf{r} = - \sum_{\mathcal{T} \in \mathcal{C}^\Omega} \left(\int_{\partial \mathcal{T}} u \mathbf{E}^{h,p} \cdot \hat{\mathbf{t}}(\ell) \, d\ell - \int_{\mathcal{T}} \hat{\mathbf{z}} \times \nabla u \cdot \mathbf{E}^{h,p} \, d\mathbf{r} \right), \quad (4.2)$$

hold $\forall \mathbf{v} \in \tilde{\mathbf{W}}^p$ and $\forall u \in \mathbf{W}^p$, respectively. Moreover, initial conditions

$$\begin{aligned} \sum_{\tilde{\mathcal{T}} \in \tilde{\mathcal{C}}^\Omega} \int_{\tilde{\mathcal{T}}} \mathbf{v} \cdot \underline{\underline{\varepsilon}} \mathbf{E}^{h,p}(\mathbf{r}, 0) \, d\mathbf{r} &= \sum_{\tilde{\mathcal{T}} \in \tilde{\mathcal{C}}^\Omega} \int_{\tilde{\mathcal{T}}} \mathbf{v} \cdot \mathbf{D}_0 \, d\mathbf{r} \quad \forall \mathbf{v} \in \tilde{\mathbf{W}}^p, \\ \sum_{\mathcal{T} \in \mathcal{C}^\Omega} \int_{\mathcal{T}} u \mu H^{h,p}(\mathbf{r}, 0) \, d\mathbf{r} &= \sum_{\mathcal{T} \in \mathcal{C}^\Omega} \int_{\mathcal{T}} u B_0 \, d\mathbf{r} \quad \forall u \in \mathbf{W}^p, \end{aligned}$$

are enforced weakly on the discrete solution. We remark that the definition of numerical fluxes is not needed to handle the non-conformity of the chosen trial spaces when discretising the (ultra-)weak curls. On boundaries where the test-functions in $\tilde{\mathbf{W}}^p$ present jumps in their tangential component, trial-functions in \mathbf{W}^p are instead tangentially continuous, and vice-versa). The following holds:

Theorem 4.1 (Consistency and stability). *Assume, for simplicity of exposition, that $H_s \equiv 0$, $\mathbf{J} \equiv \mathbf{0}$ in the rest of the section. Then, the semi-discrete formulation (4.1)–(4.2) is consistent. Furthermore the semi-discrete electromagnetic energy $\mathcal{W}^{h,p}$ stored in Ω is conserved through time:*

$$\frac{d}{dt} \mathcal{W}^{h,p} := \frac{d}{dt} \left(\frac{1}{2} \|\mathbf{E}^{h,p}\|_{\underline{\underline{\varepsilon}}}^2 + \frac{1}{2} \|H^{h,p}\|_\mu^2 \right) = 0, \quad \forall t \in (0, T), \quad (4.3)$$

where $\underline{\underline{\varepsilon}}$ and μ are piecewise-smooth inside each $K \in \mathcal{K}^\Omega$ and $\|\mathbf{E}^{h,p}\|_{\underline{\underline{\varepsilon}}} := \left(\int_{\Omega} \underline{\underline{\varepsilon}} \mathbf{E}^{h,p} \cdot \mathbf{E}^{h,p} \, d\mathbf{r} \right)^{\frac{1}{2}}$ (likewise for the magnetic field energy).

Proof. Consistency is straightforward by noting that the any sufficiently smooth solution of the continuous Maxwell system also satisfies (3.3)–(3.4). We prove (4.3). We first use the fact that our approximate solutions $H^{h,p}$ and $\mathbf{E}^{h,p}$ are themselves admissible test-functions (being linear combinations of the basis functions) and plug them as such in the weak formulation. Taking into account the simplifying assumptions, it results:

$$\sum_{\tilde{\mathcal{T}} \in \tilde{\mathcal{C}}^\Omega} \int_{\tilde{\mathcal{T}}} \mathbf{E}^{h,p} \cdot \underline{\underline{\varepsilon}} \partial_t \mathbf{E}^{h,p} \, d\mathbf{r} = \sum_{\tilde{\mathcal{T}} \in \tilde{\mathcal{C}}^\Omega} \left(- \int_{\partial \tilde{\mathcal{T}} \setminus \partial \Omega} \mathbf{E}^{h,p} \cdot H^{h,p} \hat{\mathbf{t}}(\ell) \, d\ell + \int_{\tilde{\mathcal{T}}} \nabla \times \mathbf{E}^{h,p} \cdot H^{h,p} \hat{\mathbf{z}} \, d\mathbf{r} \right), \quad (4.4)$$

$$\sum_{\mathcal{T} \in \mathcal{C}^\Omega} \int_{\mathcal{T}} H^{h,p} \mu \partial_t H^{h,p} \, d\mathbf{r} = - \sum_{\mathcal{T} \in \mathcal{C}^\Omega} \left(\int_{\partial \mathcal{T}} \mathbf{E}^{h,p} \cdot H^{h,p} \hat{\mathbf{t}}(\ell) \, d\ell - \int_{\mathcal{T}} \hat{\mathbf{z}} \times \nabla H^{h,p} \cdot \mathbf{E}^{h,p} \, d\mathbf{r} \right). \quad (4.5)$$

We now argue as follows: each $\tilde{\mathcal{T}} \in \tilde{\mathcal{C}}^\Omega$ and each $\mathcal{T} \in \mathcal{C}^\Omega$ are unions of fundamental cells. Each $K \in \mathcal{K}^\Omega$ is the support of a local term on the l.h.s. of both (4.4) and (4.5). For the r.h.s. of (4.4) instead, for any given K , there are always exactly two segments in its boundary ∂K which intersect the skeleton of the dual complex, which we label $\mathcal{S}(\tilde{\mathcal{C}}^\Omega)$. Similarly, for (4.5), there are always exactly two segments in the skeleton of the primal mesh (denoted $\mathcal{S}(\mathcal{C}^\Omega)$) which are also part of ∂K . By splitting all integrals into their contributions from each fundamental cell $K \in \mathcal{K}^\Omega$ it ensues

$$\sum_{K \in \mathcal{K}^\Omega} \int_K \mathbf{E}^{h,p} \cdot \underline{\varepsilon} \partial_t \mathbf{E}^{h,p} d\mathbf{r} = \sum_{K \in \mathcal{K}^\Omega} \left(- \int_{\partial K \cap \mathcal{S}(\tilde{\mathcal{C}}^\Omega)} \mathbf{E}^{h,p} \cdot H^{h,p} \hat{\mathbf{t}}(\ell) d\ell + \int_K \nabla \times \mathbf{E}^{h,p} \cdot H^{h,p} \hat{\mathbf{z}} d\mathbf{r} \right),$$

$$\sum_{K \in \mathcal{K}^\Omega} \int_K H^{h,p} \mu \partial_t H^{h,p} d\mathbf{r} = \sum_{K \in \mathcal{K}^\Omega} \left(- \int_{\partial K \cap \mathcal{S}(\mathcal{C}^\Omega)} \mathbf{E}^{h,p} \cdot H^{h,p} \hat{\mathbf{t}}(\ell) d\ell + \int_K \hat{\mathbf{z}} \times \nabla H^{h,p} \cdot \mathbf{E}^{h,p} d\mathbf{r} \right),$$

where we have used the homogeneous Dirichlet boundary condition for the electric field on Γ_E and for the magnetic field on Γ_H . By adding the two equations together side-by-side, for the l.h.s. it straightforwardly holds:

$$\sum_{K \in \mathcal{K}^\Omega} \int_K \mathbf{E}^{h,p} \cdot \underline{\varepsilon} \partial_t \mathbf{E}^{h,p} d\mathbf{r} + \sum_{K \in \mathcal{K}^\Omega} \int_K H^{h,p} \mu \partial_t H^{h,p} d\mathbf{r} = \frac{d}{dt} \left(\frac{1}{2} \|\mathbf{E}^{h,p}\|_{\underline{\varepsilon}}^2 + \frac{1}{2} \|H^{h,p}\|_\mu^2 \right) = \frac{d}{dt} \mathcal{W}^{h,p},$$

where we have used the assumption that time derivatives and integration in space commute. For the r.h.s. on the other hand, it holds:

$$\begin{aligned} & \sum_{K \in \mathcal{K}^\Omega} \left(- \int_{\partial K \cap \mathcal{S}(\tilde{\mathcal{C}}^\Omega)} \mathbf{E}^{h,p} \cdot H^{h,p} \hat{\mathbf{t}}(\ell) d\ell + \int_K \nabla \times \mathbf{E}^{h,p} \cdot H^{h,p} \hat{\mathbf{z}} d\mathbf{r} \right. \\ & \quad \left. - \int_{\partial K \cap \mathcal{S}(\mathcal{C}^\Omega)} \mathbf{E}^{h,p} \cdot H^{h,p} \hat{\mathbf{t}}(\ell) d\ell + \int_K \mathbf{E}^{h,p} \cdot \hat{\mathbf{z}} \times \nabla H^{h,p} d\mathbf{r} \right) = \\ &= \sum_{K \in \mathcal{K}^\Omega} \left(- \int_{\partial K} \mathbf{E}^{h,p} \cdot H^{h,p} \hat{\mathbf{t}}(\ell) d\ell + \int_K \nabla \times \mathbf{E}^{h,p} \cdot H^{h,p} \hat{\mathbf{z}} d\mathbf{r} - \int_K \mathbf{E}^{h,p} \cdot \nabla \times (H^{h,p} \hat{\mathbf{z}}) d\mathbf{r} \right) = \\ &= \sum_{K \in \mathcal{K}^\Omega} \left(- \int_{\partial K} \mathbf{E}^{h,p} \cdot H^{h,p} \hat{\mathbf{t}}(\ell) d\ell + \int_K \nabla \cdot (\mathbf{E}^{h,p} \times (H^{h,p} \hat{\mathbf{z}})) d\mathbf{r} \right) = \\ &= \sum_{K \in \mathcal{K}^\Omega} \left(- \int_{\partial K} \mathbf{E}^{h,p} \cdot H^{h,p} \hat{\mathbf{t}}(\ell) d\ell + \int_{\partial K} \mathbf{E}^{h,p} \times H^{h,p} \hat{\mathbf{z}} \cdot \hat{\mathbf{n}}(\ell) d\ell \right) = 0 \end{aligned}$$

where we have used the trivial fact $\partial K = \{\partial K \cap \mathcal{S}(\tilde{\mathcal{C}}^\Omega)\} \cup \{\partial K \cap \mathcal{S}(\mathcal{C}^\Omega)\}$ (i.e. the union of four segments), the fact that $\hat{\mathbf{z}} \times \nabla H^{h,p} = \nabla \times (H^{h,p} \hat{\mathbf{z}})$ and where the last two lines then follow by using elementary vector calculus, the divergence theorem on locally smooth functions on each K and by applying the definition (2.4). The present proof can be easily extended to the general case where H_S and \mathbf{J} are not identically zero with minor additional details. \square

Finally, finding bases for the spaces $\tilde{\mathbf{W}}^p$ and \mathbf{W}^p is not a trivial task, and we refer the reader to Appendix A, where such an explicit construction is given in detail. We can here just assume such bases $\{\tilde{\mathbf{w}}_n^p\}_{n=1}^N$ and $\{w_m^p\}_{m=1}^M$ are given. We can thus expand the approximated unknown fields as

$$\mathbf{E}^{h,p}(\mathbf{r}, t) = \sum_{n=1}^N u_n(t) \tilde{\mathbf{w}}_n^p(\mathbf{r}), \quad H^{h,p}(\mathbf{r}, t) = \sum_{m=1}^M f_m(t) w_m^p(\mathbf{r}), \quad (4.6)$$

where the space-time separation of variables assumption on the solution is incorporated via the time dependence of coefficients in the linear combinations. The following then additionally holds:

Corollary 4.2. *The semi-discrete scheme, which we obtain by using (4.6) and testing (4.1)–(4.2) against the same basis functions, has the following matrix-representation:*

$$\begin{pmatrix} \tilde{\mathbf{M}}_p^\varepsilon & \mathbf{0} \\ \mathbf{0} & \mathbf{M}_p^\mu \end{pmatrix} \frac{d}{dt} \begin{pmatrix} \mathbf{u}(t) \\ \mathbf{f}(t) \end{pmatrix} = \begin{pmatrix} \mathbf{0} & \mathbf{C}_p^\top \\ -\mathbf{C}_p & \mathbf{0} \end{pmatrix} \begin{pmatrix} \mathbf{u}(t) \\ \mathbf{f}(t) \end{pmatrix}, \quad (4.7)$$

where \mathbf{f} is the column-vector containing semi-discrete magnetic field degrees of freedom (DoFs), \mathbf{u} is the column-vector containing semi-discrete electric field DoFs, and where the energy conservation property is reflected by the r.h.s. skew-symmetry.

Proof. The proof is constructive: it suffices to perform again all the steps of Theorem 4.1, using as test and trial function for the electric field any basis function for the space $\tilde{\mathbf{W}}^p$ and as a test and trial function for the magnetic field any basis function for the space \mathbf{W}^p . Alternatively, one can take the l.h.s. of any of the two equations, again for a single pair of trial and test function and perform elementary manipulations to show that it coincides with the transpose of the remaining weak equation. \square

5. The discrete scheme as a high order cell method

To discretise time, we use the well-known leap-frog scheme, which is the symplectic time-integrator used by Yee in his seminal paper. The search for symplectic integrators of arbitrary order which keep the time-stepping explicit is an active topic of research (see [36–38]) which goes beyond the scope of the present contribution (yet provides also a further future research direction). For the fully discrete scheme it ensues

$$\begin{pmatrix} \mathbf{u}^{(n+1/2)} \\ \mathbf{f}^{(n+1)} \end{pmatrix} = \begin{pmatrix} \mathbf{u}^{(n-1/2)} \\ \mathbf{f}^n \end{pmatrix} + \Delta t \begin{pmatrix} (\tilde{\mathbf{M}}_p^\varepsilon)^{-1} & \mathbf{0} \\ \mathbf{0} & (\mathbf{M}_p^\mu)^{-1} \end{pmatrix} \begin{pmatrix} \mathbf{0} & \mathbf{C}_p^\top \\ -\mathbf{C}_p & \mathbf{0} \end{pmatrix} \begin{pmatrix} \mathbf{u}^{(n+1/2)} \\ \mathbf{f}^n \end{pmatrix}, \quad (5.1)$$

where $\Delta t \in \mathbb{R}^+$ is the discrete time-step (whose upper bound for a stable scheme can quickly be estimated by, e.g., a power-iteration algorithm) and $n = 0, 1, 2, \dots, \lceil T/\Delta t \rceil$, \mathbf{f}^n is the column-vector containing (now fully discrete) magnetic field DoFs at time $t = n\Delta t$ and $\mathbf{u}^{(n+1/2)}$ is the column-vector containing electric field DoFs, computed at time $t = (n+1/2)\Delta t$. Since the spaces are non-conforming, basis functions will conveniently have compact support limited to one triangle or one dual cell (depending on the unknown). The final system will therefore be explicit in time, since the inverses of mass-matrices are easily computed and stored by solving very small local systems of equations, once-and-for-all and block-by-block. To visualize this feature we refer the reader to the sparsity patterns in Fig. 2 and Fig. 3 (which are relative to the mass-matrices derived from bases constructed in Appendix A).

It is known that, both for conforming discretisations relying on finite elements of the Nedelec [6] type and for DG formulations based on central fluxes, the requirement is to have basis functions which are piecewise-polynomials of degree p and $p+1$ for the magnetic and electric field respectively (or vice-versa). This leads to sub-optimal convergence rates in the electromagnetic energy norm and also implies that, for the lowest admissible order, we need basis functions which are piecewise-affine for one of the two unknown fields. For the proposed method instead, the two unknowns are approximated up to the same polynomial degree, and the lowest admissible one is $p=0$, i.e. piecewise-constant fields.

Specifically, in the case $p=0$, we are left with one degree of freedom (DoF) per triangle for the scalar $H^{h,0}(\mathbf{r}, t)$ and two DoFs per each triangle edge in the primal complex for the vector field $\mathbf{E}^{h,0}(\mathbf{r}, t)$. A simple illustrating example is given in Fig. 4 for a mesh consisting of two triangles \mathcal{T}_1 and \mathcal{T}_2 : we have there ten DoFs for the electric field $u_{n=1,2,\dots,10}$ and two DoFs (one per triangle) for the magnetic field $f_{m=1,2}$. Their indexing is induced strictly from the ordering of vertices in the primal complex: it is easy to prove that the $\mathbf{u}(t)$ DoFs are line-integrals of the electric fields along bisected edges in $\mathcal{S}(\mathcal{C}^\Omega)$ while the $\mathbf{f}(t)$ DoFs are fluxes of the $B^{h,0}(\mathbf{r}, t) := \mu H^{h,0}(\mathbf{r}, t)$ scalar field across the triangles $\mathcal{T} \in \mathcal{K}^\Omega$.

The discrete operator \mathbf{C}_0 and its transpose are instead exactly incidence matrices: this result (already shown in [31]) can be proved by direct computation (see formula (B.2) in Appendix, where, as the reader may notice, the area integrals vanish identically, since $p=0$, but line-integrals do not). The left-multiplication of DoFs vectors with the incidence matrix $\mathbf{C}_0 \mathbf{u}$ equates to the Stokes theorem:

$$\int_{\mathcal{T}_m} \partial_t(\mu H^{h,0}) d\mathbf{r} = \oint_{\partial \mathcal{T}_m} \mathbf{E}^{h,0} \cdot \hat{\mathbf{t}}(\ell) d\ell, \quad m = 1, 2, \dots, |\mathcal{C}^\Omega|,$$

where we again shall stress that the $\mathbf{E}^{h,0}(\mathbf{r}, t)$ field is allowed to be fully discontinuous on the dashed dual edges.

We remark that this is exactly the Cell Method's framework advocated by Tonti [19,20], while also being a generalization of the Yee algorithm to unstructured meshes. The peculiarity of having to split each edge in \mathcal{C}^Ω into two segments (while still preserving the physical interpretation of DoFs) is also not new, but was instead studied by some of the authors in the 3D setting in [21,23,39], where tetrahedral meshes were used. In fact the lowest order basis functions for the proposed method are piece-wise constant one-forms which coincide exactly with the basis functions introduced in [21].

6. Numerical results

We shall here validate the method through numerical experiments. All computations are in natural units, i.e. physical units have been rescaled such that the speed of light in a vacuum is normalized to one, which means in practice $\varepsilon = \varepsilon_r$ and $\mu = \mu_r$.

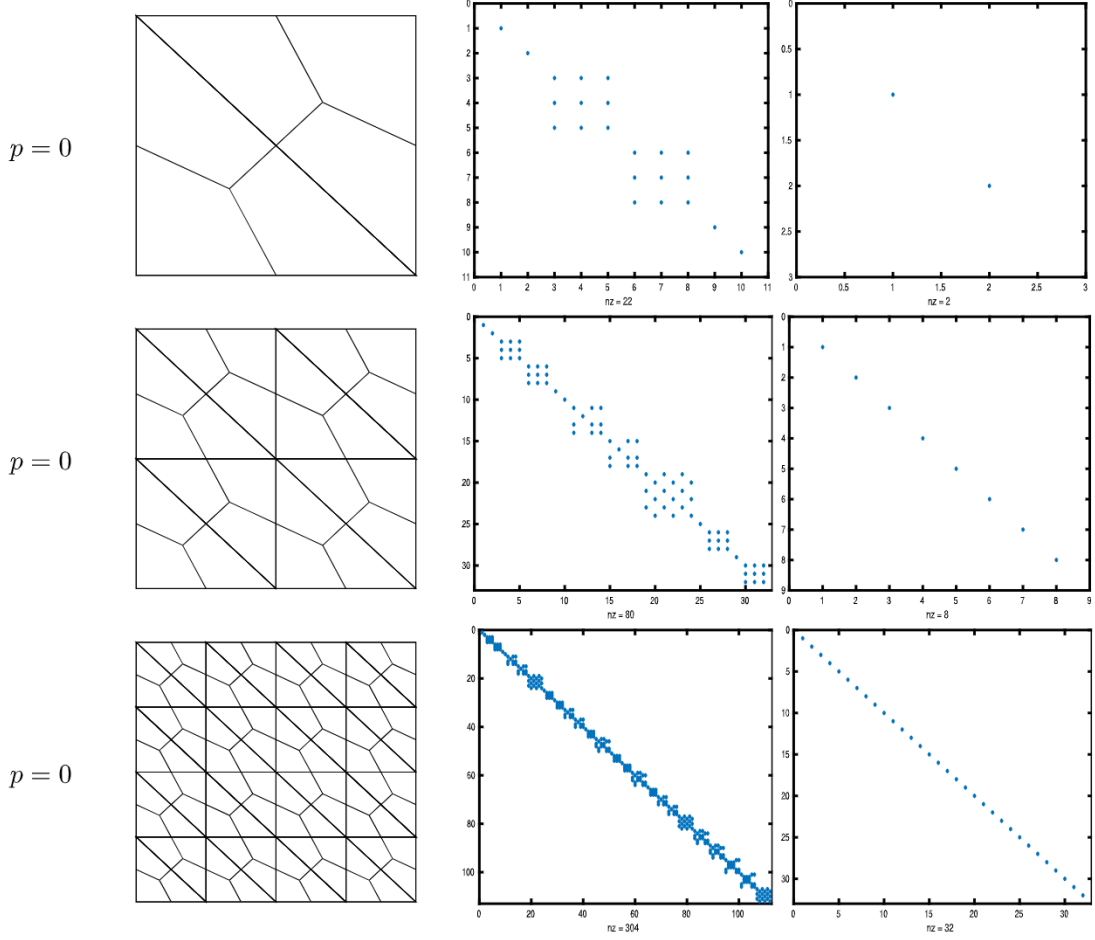


Fig. 2. The sparsity pattern for the lowest order \mathbf{M}_0^e (second column) and \mathbf{M}_0^μ (third column) under uniform h -refinement, i.e. meshes in the first column are constructed by barycentric duality of uniform refinements (by means of edge-bisection) of the starting primal C^Ω mesh. The label nz denotes the number of non-zero entries. Since for $p=0$ only \tilde{w}_T functions survive for the $H^{h,p}$ field, \mathbf{M}_0^μ is fully diagonal.

6.1. MIBVP results

To test the transient behaviour of the method we use a manufactured time domain problem, with solution already available in closed form in [23], where the computational domain is a waveguide $\Omega = (0, 1) \times (0, 2)$. The fundamental propagating mode² is enforced as a time-dependent boundary condition $E_s(x, t) = \sin(\pi * x) \sin(\omega t)$ at the entrance $y = 0$ of the waveguide, while all other segments in $\partial\Omega$ are set to perfect electric conductor (PEC). To simulate an invariant structure in the z direction (a needed assumption for true 2D problems) we need a transverse-electric (TE) mode, i.e. only one component of the electric field is not identically zero. It is very convenient for the purpose to swap the field approximation spaces with respect to the theory and make the \mathbf{E} field a pseudo-vector. This poses no real hardships, as the input field can be injected as an equivalent magnetic current by projecting it on the vector-valued trial-space (which requires 1D Gauss integration on mesh edges at $y = 0$).

The behaviour in the whole waveguide for the three non-zero components of the electromagnetic field is shown in Fig. 5, for polynomial degree $p = 5$, average mesh size $h = 0.2$ and at time $t = 2$ (again in natural units). Due to the reflections at $y = 2$, the z -aligned field is not everywhere continuously differentiable in time. The presence of critical points in the temporal behaviour is visible in Fig. 6, which shows how the various polynomial orders behave for the same mesh, chosen to be rather coarse with a maximum mesh size of $h = 0.2$. All polynomial degrees in the bases are tested with the leap-frog time-stepping scheme using Δt equal to the upper limit for stability (the usual practical choice). The qualitatively better approximation properties of the higher order versions of the method are clearly visible.

At the current stage, we do not make any claim to have programmed the fastest possible version of the method, yet it is useful to remark that for $p = 6$ and the above mentioned average mesh size $h = 0.2$, the method requires 21 472 DoFs (6 464

² the waveguide-mode with the lowest cut-off frequency.

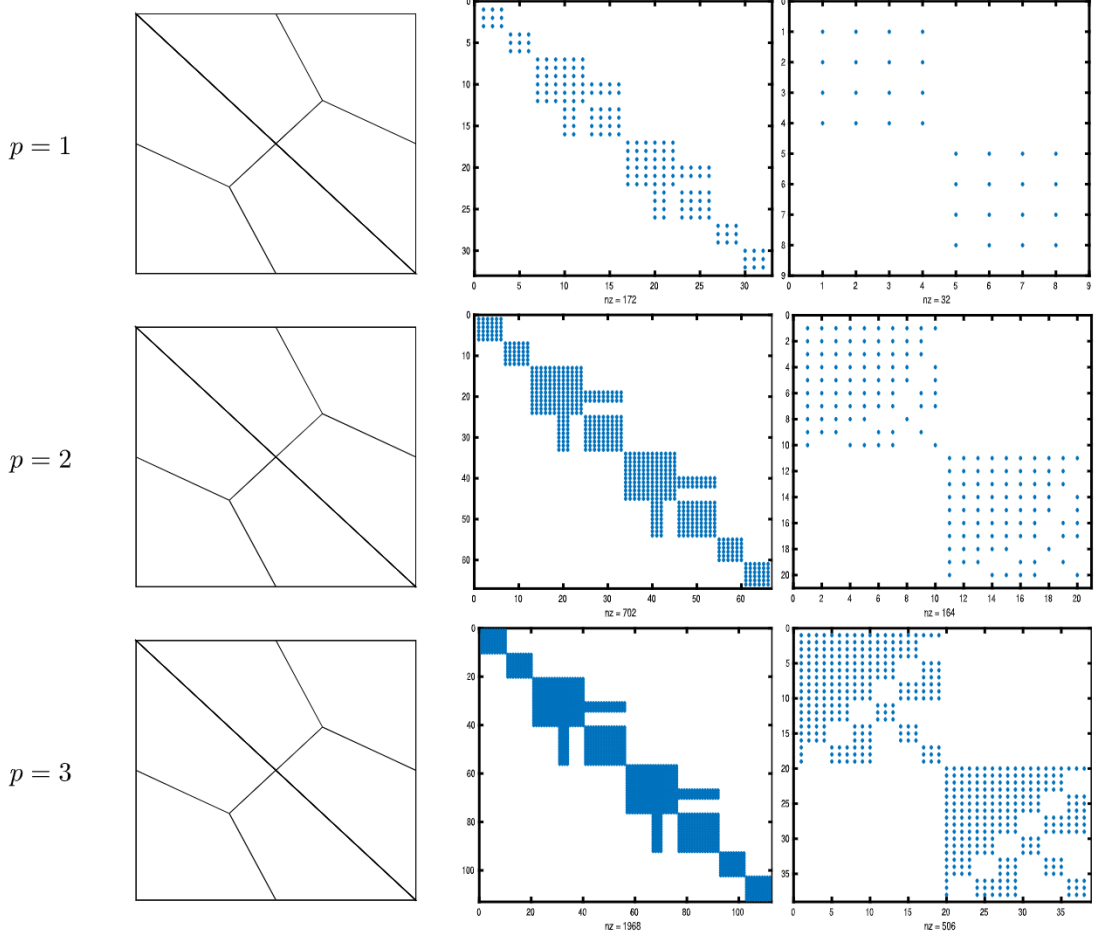


Fig. 3. The sparsity pattern for the mass-matrices $\tilde{\mathbf{M}}_p^e$ (second column) and \mathbf{M}_p^u (third column) can also be studied under uniform p -refinement, i.e. the meshes remain unchanged in size, but the polynomial order is increased, namely we have $p = 1, 2, 3$. The label nz again denotes the number of non-zero entries.

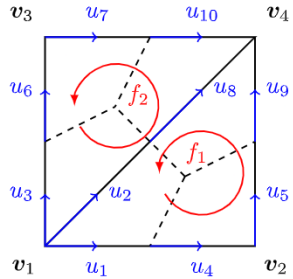


Fig. 4. The $p = 0$ method at work on a mesh consisting of two triangles T_1 (with vertices v_1, v_2, v_4) and T_2 (with vertices v_1, v_3, v_4). We note that PEC boundary conditions can be strongly enforced, owing to the nature of the discrete DoFs for \mathbf{W}^0 .

for the scalar-valued unknown, 15 008 for the vector-valued one), the maximum allowed time-step is $\Delta t = 3.833 \times 10^{-3}$, and the computation reaches a yield of 129.633 time-steps per second (in wall-time, averaged over simulations with 10^5 time-steps) on a modest laptop computer (Intel Core i7-6500U CPU, clocked at 2.50 GHz with 4 physical cores, 8 GB of RAM), which amounts to roughly 2.783×10^6 DoFs/second of average performance.

6.2. Spectral accuracy

Due to low regularity of the true solution for the transient waveguide problem, we cannot expect to observe the theoretical order of convergence for the method. A good way to assess the superiority in terms of approximation properties when

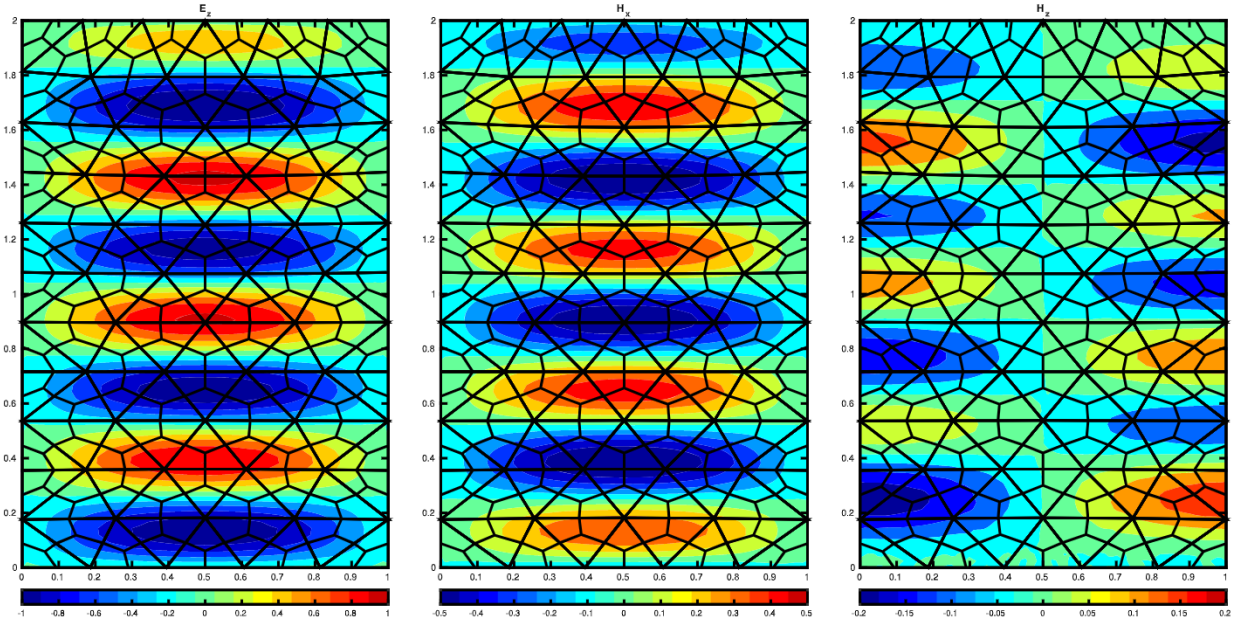
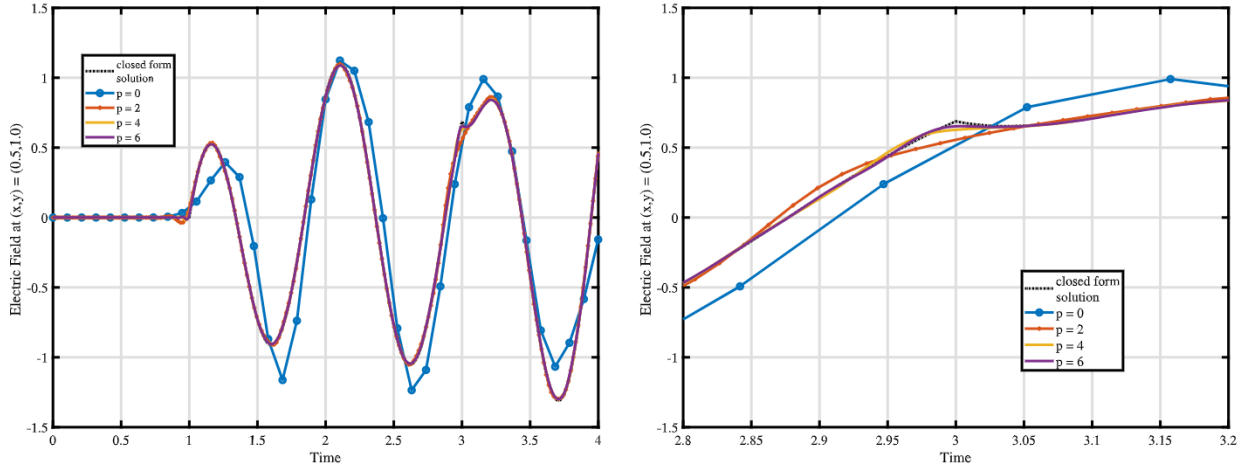
Fig. 5. The transient field in the waveguide at $t = 2$.

Fig. 6. The left panel shows the time-dependent solution to the waveguide problem. The field is measured at the centroid of the domain, as can be inferred by the delay in the propagation at the start. In the right panel a blow-up of a small interval around $t = 3.0$ is shown, where a critical point in the solution must be approximated.

using higher order basis functions is to use the proposed method to solve an associated generalized eigenvalue problem. In fact, since we are using a kind of discontinuous Galerkin approach, the spectral accuracy of the method is interesting in its own right, and not just as a mean to study convergence, since we have no formal guarantee for the absence of spurious modes, which would tarnish the appeal of any new numerical method. By acting directly on the semi-discrete system of (4.7) and making it time-harmonic ($\partial_t \mapsto -i\omega$, where $i = \sqrt{-1}$) we arrive at the two following “dual” formulations:

$$\mathbf{C}_p(\mathbf{M}_p^\varepsilon)^{-1} \mathbf{C}_p^T \hat{\mathbf{f}} = \lambda \mathbf{M}_p^\mu \hat{\mathbf{f}}, \quad (6.1)$$

$$\mathbf{C}_p^T (\mathbf{M}_p^\mu)^{-1} \mathbf{C}_p \hat{\mathbf{u}} = \lambda^* \mathbf{M}_p^\varepsilon \hat{\mathbf{u}}, \quad (6.2)$$

where the hat super-script denotes the time-harmonic solutions and λ, λ^* are the squared eigenfrequencies. Depending on boundary conditions, (6.1)–(6.2) approximate either the Dirichlet MEP or the Neumann one. We choose to work with (6.1) since in two dimension we are thus basically approximating the Laplace operator with the matrix $\mathbf{C}_p(\mathbf{M}_p^\varepsilon)^{-1} \mathbf{C}_p^T$.

As a first example we take the unit square domain $\Omega = (0, 1) \times (0, 1)$ with uniform material coefficients $\mu_r = 1$ and $\varepsilon_r = 1$. In this case the eigenvalues are of the form $\lambda = (a^2 + b^2)\pi^2$ where $a, b \in \mathbb{N}^+$ for Dirichlet boundary conditions on the H field and $a, b \in \mathbb{N}_0$ for Neumann ones.

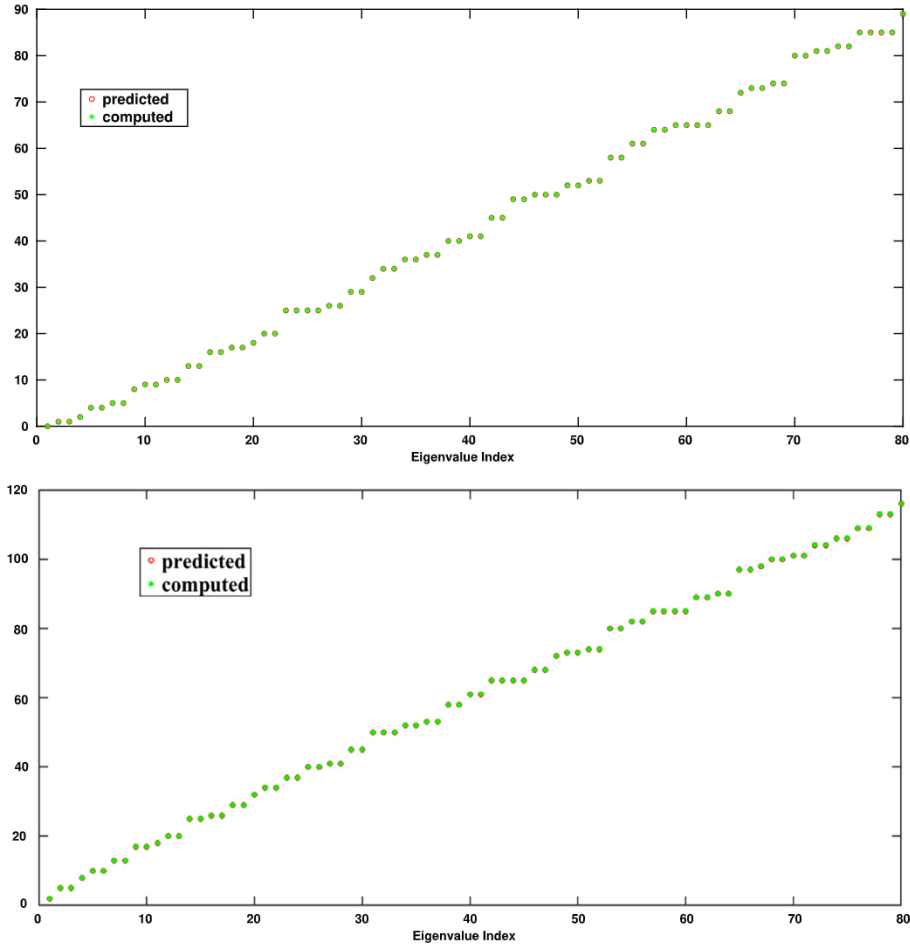


Fig. 7. We show spectral correctness of the proposed method when solving the generalized eigenvalue problem in (6.1) for Neumann (note the one zero eigenvalue in the upper panel), and Dirichlet boundary conditions in lower panel. Here $\mu_r = \varepsilon_r = 1$ holds on the whole domain Ω .

Fig. 7 shows the first 80 eigenvalues (all scaled by π^2) for both cases, computed with $p = 4$ and $h = 0.2$ using the **eigs** function [40] in MATLAB. No spurious eigenvalues appear (we note there is exactly one zero eigenvalue for the Neumann problem). Thorough testing for all $p < 8$ and various mesh sizes corroborates the absence of spurious eigenmodes due to the method. The accuracy is quite impressive for the shown test, for which we also present the first ten computed eigenfunctions in Fig. 10, where we note that, when the associated eigenvalue has algebraic multiplicity bigger than one, we cannot easily force the chosen solver to yield the appropriate mutually orthogonal eigenfunctions instead of a pair of their linear combinations.

A more formal study of convergence is shown in Fig. 8, which reveals $\mathcal{O}(h^{2p})$ convergence when polynomial degree p is used and the mesh-size h vanishes. This has been found to hold for the eigenvalues of both generalized problems (6.1)–(6.2). The obtained rates are in agreement with the theoretical studies of Buffa & Perugia in [41] for DG methods. We nevertheless stress that the analysis therein relies on the introduction of (mesh and polynomial degree dependent) penalty parameters, which should be big enough to ensure coercivity of the bilinear form in the l.h.s. of the weak formulation of the eigenvalue problem. No free parameters are instead present in the herein proposed formulation. We furthermore remark that the $p = 0$ version of the method shows $\mathcal{O}(h^{2p+2})$ convergence rate, but this super-convergence phenomenon is not sustained with higher polynomial degrees, at least for the proposed sets of basis functions. This fact clearly begs for further theoretical investigation.

Contextually, we tested the convergence in the L^2 norm on the numerical approximation of the associated eigenfunctions. We observe the optimal convergence rate $\mathcal{O}(h^{p+1})$ under h -refinement for all the tested polynomial degrees, as shown in Fig. 9. We remark that in classical DG schemes the optimal rate is achieved only in the case of upwinding schemes, which sacrifice energy conservation (see [42]). On the other hand it must be noted that, for the same mesh, the presented method yields more unknowns than fully discontinuous approximations, by a factor which, in two dimensions, grows from one to three (asymptotically) with increasing polynomial degree in the bases (due to the presence of the dual complex). Our first investigations suggest that this apparent drawback is decisively mitigated by the improved accuracy of the method. Nevertheless more thorough comparisons with all the competing DG approaches in terms of accuracy versus number of

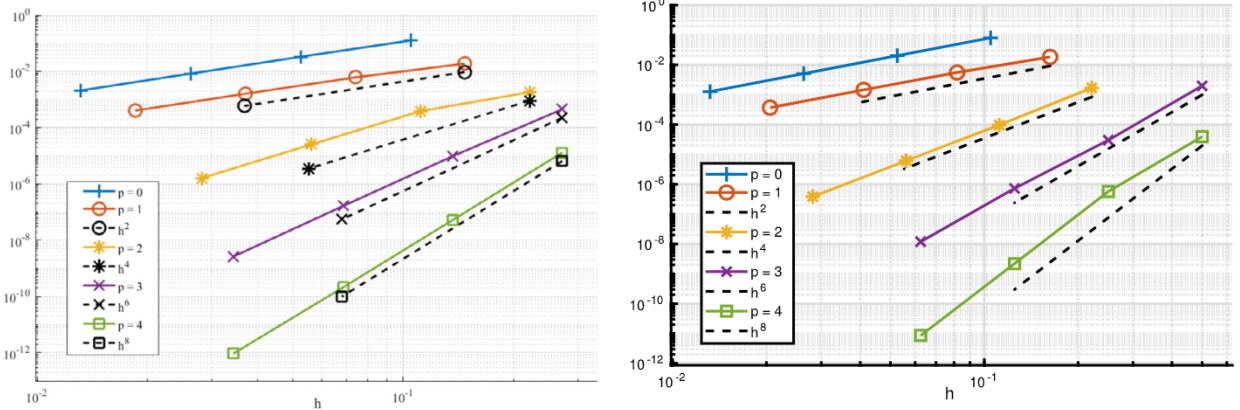


Fig. 8. The error in approximating the 20th eigenvalue of the Dirichlet (left panel) and Neumann (right panel) problem with respect to the mesh size h vanishes with the expected rate for the various tested polynomial orders p for the case of a uniformly filled cavity.

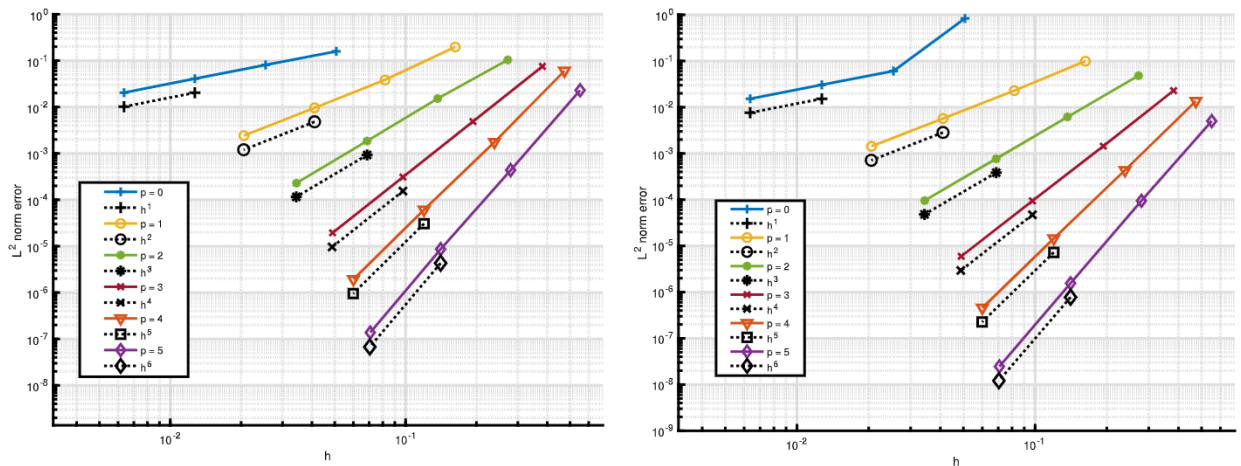


Fig. 9. The L^2 error for the associated eigenfunction (with respect to Fig. 8): Dirichlet (left) and Neumann (right) problems.

unknowns (also taking into account the delicate role of penalty parameters in competing algorithms) would undoubtedly provide valuable information. Such studies are being carried out and will be reported elsewhere.

As a more testing setup, we split our square Ω exactly into two halves, with a discontinuity aligned with the y axis. We fill the left half of the cavity $\Omega_1 = (0, 1/2) \times (0, 1)$ with a higher index material $\varepsilon_1 = 4$, which corresponds to halving the speed of light with respect to the vacuum parameters, which we keep intact on $\Omega_2 = \Omega \setminus \Omega_1$. The exact values of the Neumann eigenvalues are not easily computable with pen and paper any more, as one needs to solve a transcendental equation (see [43]) involving hyperbolic functions. Yet, using any symbolic mathematics toolbox, we can estimate their values with arbitrary precision. We show the first ten eigenfunctions we computed (again with $p = 4$ and $h = 0.2$) as a reference in Fig. 11, where we stress the fact that “partially evanescent” modes appear in the spectrum: more formally these are modes with real wave-number $k = (k_x^2 + k_y^2)^{1/2}$ (due to the positive-definiteness property of the considered operator) despite having imaginary k_x . This behaviour is confirmed by the distribution of eigenvalues in Fig. 12 (leftmost panel, which again shows no spurious solutions), where the eigenvalues are shown to be perturbed closer together towards zero. The optimal order of convergence with varying polynomial degree is also again confirmed for the discontinuous material case in Fig. 12 (right panel).

As a final test we show how the method behaves when singular solutions are expected. To this end we use the celebrated L -shaped domain: $\Omega = \{(-1, 1) \times (-1, 1)\} \setminus \{(0, 1) \times (-1, 0)\}$, for which the first six eigenfunctions when solving the Neumann problem are shown in Fig. 13, computed with a fine mesh. We show the six associated eigenvalues in 14, where values from [44] (numerically estimated with the standard FEM, with eleven digits expected to be correct) are taken as a reference solution. Again no spurious solutions are observed. Naturally, optimal convergence cannot be expected (at least not with a naive mesh-refinement strategy) for the second and for the sixth eigenvalue, as the associated eigenfunctions have a strong unbounded singularity at the origin. Restoring optimal convergence by appropriate hp -refinement goes outside of the scope of the present contribution, while again providing an obvious research direction for future work.

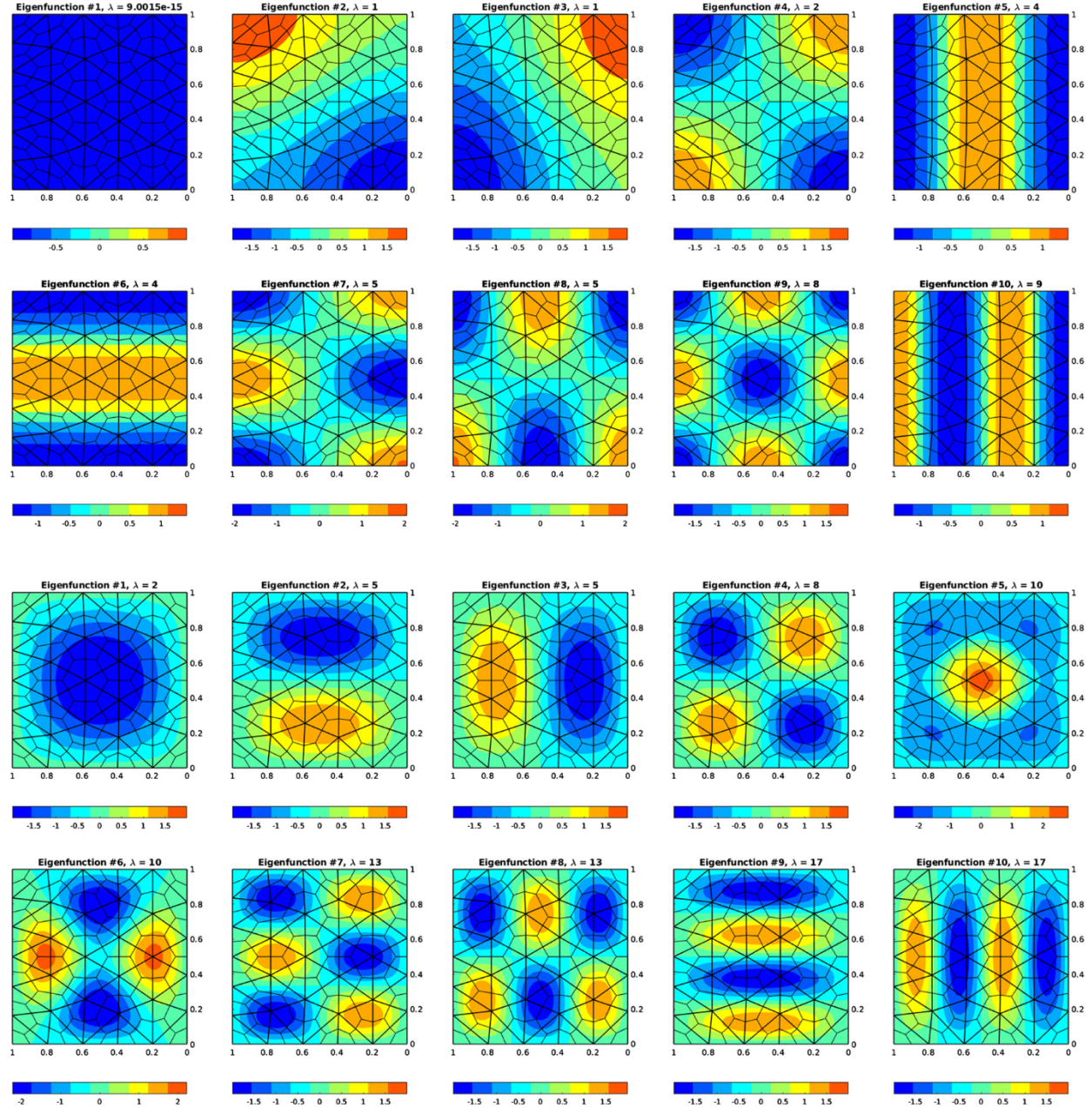


Fig. 10. The first ten computed eigenfunctions for the case of the uniformly filled cavity: Neumann and Dirichlet case.

7. Conclusions

The proposed method presents very promising approximation properties, as shown both by theoretical and numerical investigations. Its potential for high-performance is preserved by the block-diagonal structure of the mass-matrices. Furthermore, the arbitrary order version also preserves the explicit splitting of the involved discrete operators into topological and geometric ones. It has also not escaped our notice that, with slight modifications in the definitions of shape-functions and transformation rules, a method applicable to the acoustic wave equation (in the velocity-pressure first order formulation) instead of the Maxwell system can be obtained. In lack of a complete theory, we hope that its extension to three spatial dimensions, which is currently being carried out and will be the topic of a future submission, will further show its effectiveness as a fast solver for the time-dependent Maxwell equations. Nevertheless, a more thorough theoretical analysis for the introduced functional spaces and the development of a spectral theory for the involved operators is a mandatory question to be investigated by researchers.

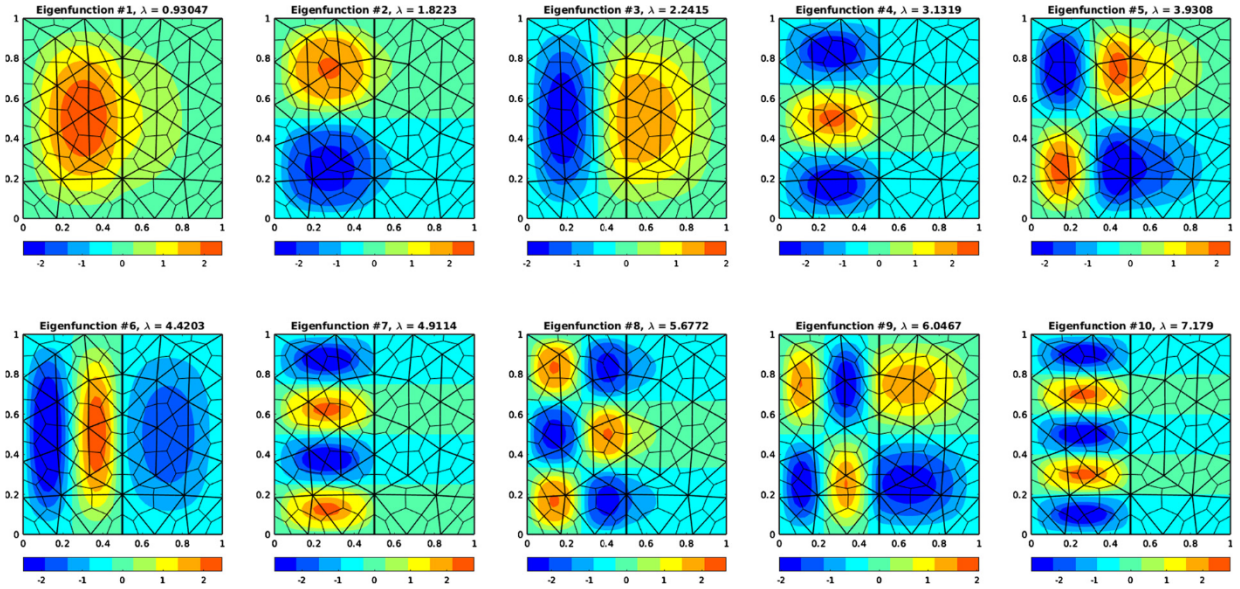


Fig. 11. Eigenfunctions for the cavity with discontinuous permittivity.

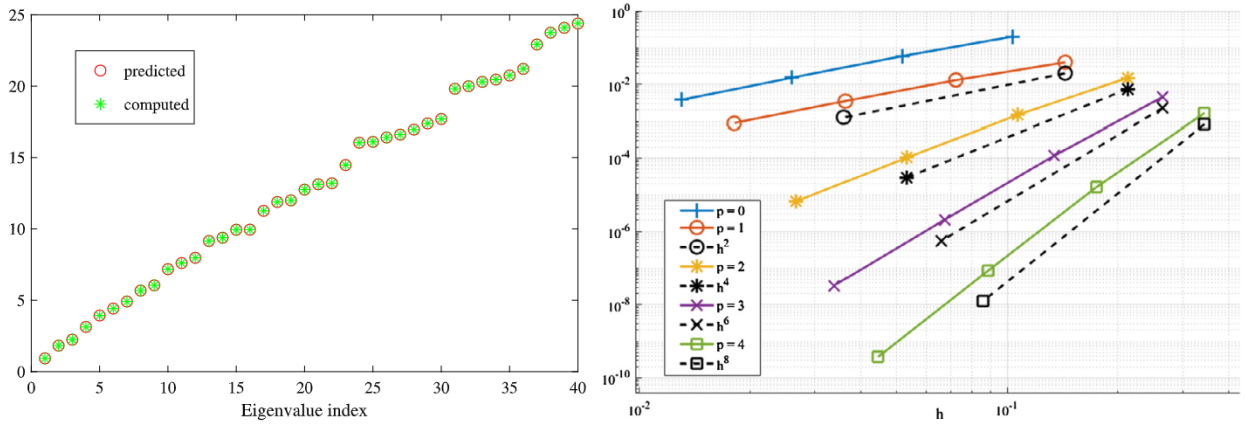


Fig. 12. The method remains spectrally correct when approximating the Neumann problem for the inhomogeneously filled square. The error in approximating the 20th eigenvalue is shown on the right to also still vanish with the optimal rate, with respect to the mesh size h , for the various tested polynomial orders p .

On a more critical note, we remark that the proposed local shape-functions, although in principle of arbitrary degree and hierarchical, are not practical for polynomial degrees $p > 5$, since bases consisting of scaled monomials on a subset of the unit square will quickly yield ill-conditioned mass-matrix blocks (see also [45]). This can be mended by partial orthonormalization techniques which do not pose any drastic theoretical hardships.

We finally remark that a reduction of the present high-order method to Cartesian-orthogonal meshes is straightforward (via the same barycentric-dual procedure), and the resulting scheme degenerates to Yee's algorithm when piecewise-constant bases are used. On the other hand, the presented approach can be applied in principle to generic polytopal meshes, due to its more general variational statement. This insight provides another possible direction for future work.

CRediT authorship contribution statement

The authors have contributed in the following way: All three authors have contributed to the conceptualization and Methodology development of the presented material. Authors L.C. and B.K. carried out the theoretical analysis, and have programmed the software used for the shown results, which were obtained by simulations done by author B.K. which also curated the data obtained and produced the manuscript. Authors L.C. and J.S. reviewed and supervised its form. Author J.S. obtained funding which supported author B.K. during much part of the work.

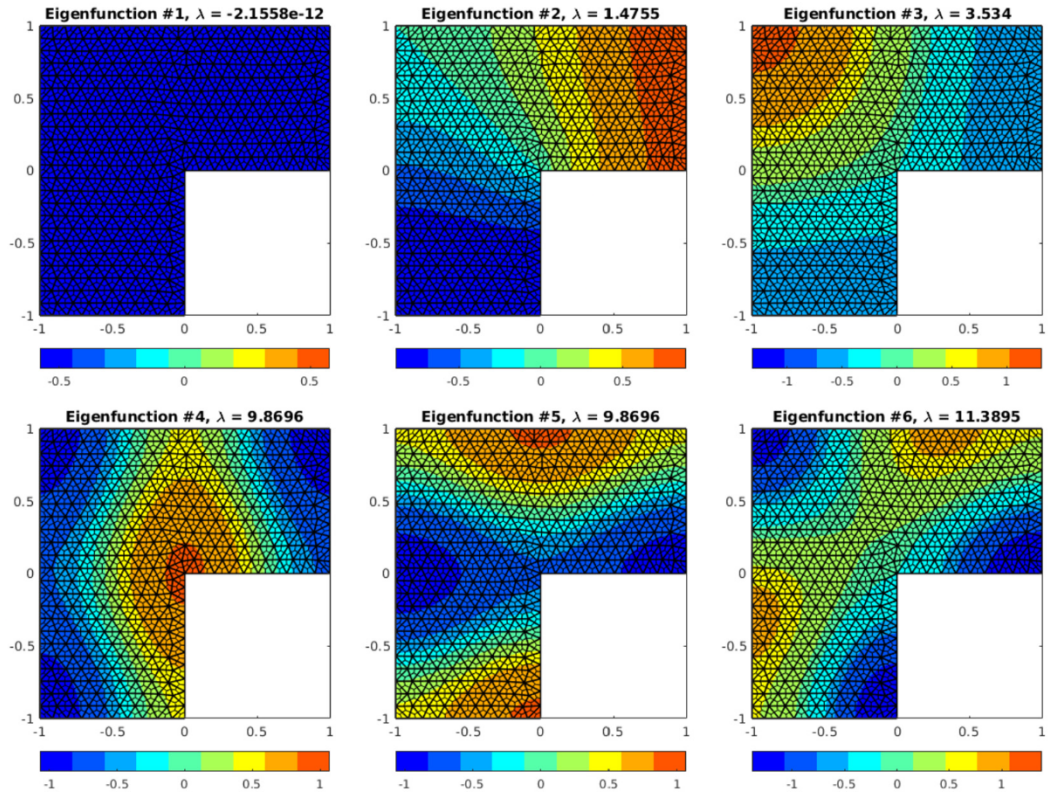
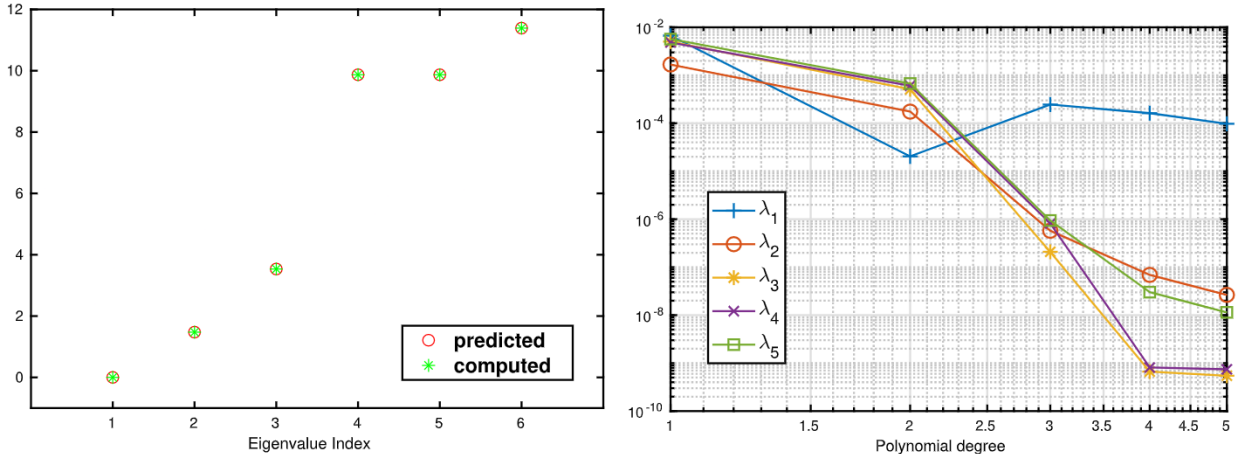


Fig. 13. The first six eigenfunctions for the L-shape domain.

Fig. 14. Spectral correctness check for the L-shape domain: first six eigenvalues (on the left). On the right we show convergence under p refinement for the approximation of the first five non-zero eigenvalues.

Declaration of competing interest

The authors declare that they have no known competing financial interests or personal relationships that could have appeared to influence the work reported in this paper.

Acknowledgements

Author Bernard Kapidani was partially financially supported by the Austrian Science Fund (FWF) under grant number F65: *Taming Complexity in Partial Differential Equations*. All authors would like to thank the anonymous reviewer, whose suggestions and questions led to a vastly improved paper.

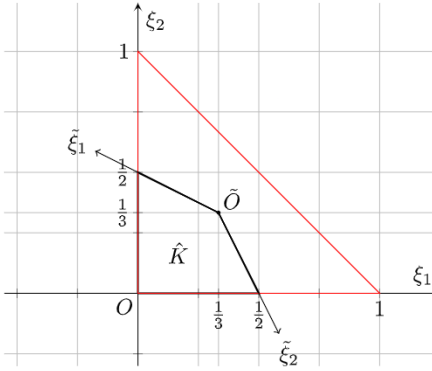


Fig. 15. The reference kite-cell and the reference triangle, from which it is derived.

Appendix A. Explicit construction of basis functions

Let us start by defining local Cartesian-orthogonal coordinates (ξ_1, ξ_2) and denote with $\hat{\mathcal{T}}$ the reference (or master) triangle, i.e. the convex hull of the point-set $\{(0,0)^\top, (1,0)^\top, (0,1)^\top\}$ in the given coordinates. We will denote with $\hat{\mathbf{r}} = \hat{\mathbf{r}}(\xi_1, \xi_2)$ position vectors on $\hat{\mathcal{T}}$. In standard FEM, the procedure usually consists in defining local “shape-functions” on $\hat{\mathcal{T}}$ and subsequently using a family of continuous and invertible mappings $\varphi_{\mathcal{T}}$ (which map $\hat{\mathcal{T}}$ to each physical triangle $\mathcal{T} \in \mathcal{C}^\Omega$) to “patch-up” global basis functions on the whole of Ω . However, we note that there are, for each $\mathcal{T} \in \mathcal{C}^\Omega$, actually three different choices for affine transformations which map vertices of $\hat{\mathcal{T}}$ to vertices of \mathcal{T} (up to reversal of orientation, depending on which angle of the triangle is the image of the right angle of $\hat{\mathcal{T}}$), and they are in the form:

$$\mathbf{r} = \varphi_{\mathcal{T},i}(\hat{\mathbf{r}}) := \mathbf{A}_{\mathcal{T},i}\hat{\mathbf{r}} + \mathbf{b}_{\mathcal{T},i},$$

where $i \in \{1, 2, 3\}$, $\hat{\mathbf{r}} \in \hat{\mathcal{T}}$, $\mathbf{r} \in \mathcal{T}$, $\mathbf{A}_{\mathcal{T},i} \in \mathbb{R}^{2 \times 2}$, $\mathbf{b}_{\mathcal{T},i} \in \mathbb{R}^2$. If we take any triangle $\mathcal{T} \in \mathcal{C}^\Omega$, denote with $\mathbf{v}_{\mathcal{T},1}, \mathbf{v}_{\mathcal{T},2}, \mathbf{v}_{\mathcal{T},3}$ the Euclidean vectors (now in the global mesh coordinates) for the three vertices in the set $\{\partial\mathcal{T} \cap \mathcal{V}^\Omega\}$ (with \mathcal{V} set of vertices of \mathcal{C}^Ω), and we recall that (as already remarked) each pair $(T, \mathbf{v}_{\mathcal{T},i})$ uniquely identifies a quadrilateral $K \in \mathcal{K}^\Omega$, we can make the notation less cumbersome by writing φ_K (and $\mathbf{A}_K, \mathbf{b}_K$ as well) instead of using two subscripts. In connection with this, the following result additionally holds:

Lemma A.1. For each $\mathcal{T} \in \mathcal{C}^\Omega$, $\{\mathbf{v}_{\mathcal{T},i}\}_{i=1,2,3}$ (defined as above), the affine mapping $\varphi_{\mathcal{T},i} := \varphi_K$ is invertible, and the inverse φ_K^{-1} maps $K \in \mathcal{K}^\Omega$ to the kite³-cell (KC), denoted with \hat{K} and defined as

$$\hat{K} = \text{Conv} \left\{ (0,0)^\top, (1/2,0)^\top, (1/3,1/3)^\top, (0,1/2)^\top \right\},$$

where $\text{Conv}\{\cdot, \dots, \cdot\}$ denotes the convex hull of its arguments. \square

Here lies in fact our biggest departure from the classical FEM approach: we work on a proper subset of the reference triangle $\hat{\mathcal{T}}$, namely \hat{K} . Both $\hat{\mathcal{T}}$ and \hat{K} are depicted in Fig. 15.

We can still work with the exact same local set of coordinates (ξ_1, ξ_2) and define the following shape-functions’ set:

$$\hat{\mathbf{w}}_l^{ij}(\hat{\mathbf{r}}) = C_{ijl}(\xi_l)^i (\xi_{3-l})^j \hat{\nabla} \xi_l, \quad l \in \{1, 2\}, \quad i, j \geq 0, \quad i + j \leq p, \quad (\text{A.1})$$

where i, j are integers, and $\hat{\nabla}$ denotes the gradient operator in the local coordinates. The values of scaling factors $C_{ijl} \in \mathbb{R}^+$ ensure that shape-functions assume all values in $(0, 2)^2$ for some $\hat{\mathbf{r}} \in \hat{K}$.

We remark that local shape-functions defined in (A.1) are of two kinds. For example, by setting $j = 0$ we get “edge” functions, in the following sense: the selected shape-functions yield monomials in arc-length when their tangential component is computed on the line $\xi_l = 0$ and yield zero when their tangential trace is computed on $\xi_{3-l} = 0$. This is a useful property when mapping vector-valued functions back to the *physical* element $K \in \mathcal{K}^\Omega$. To do so we have to digress shortly on the index l , which is in fact a function of two additional indices: we can write (with some harmless abuse of notation in identifying sets with their indexing) $l = l(e, K)$, for any $e \in \mathcal{S}(\mathcal{K}^\Omega) \cap \mathcal{S}(\mathcal{C}^\Omega)$ and any $K \in \mathcal{K}^\Omega$ s.t. $e \subset \partial K$. This completely specifies which one of the local coordinates (ξ_1, ξ_2) provides an arc-length parametrization for the image of segment e (under the appropriate mapping φ_K^{-1}) and allows us to introduce the set of functions:

³ a quadrilateral where two disjoint pairs of adjacent sides are equal.

$$\tilde{\mathbf{w}}_e^i(\mathbf{r}) := \begin{cases} \mathbf{A}_K^{-T} \hat{\mathbf{w}}_l^{i0}(\varphi_K^{-1}(\mathbf{r})), & \forall \mathbf{r} \in K, \forall K \in \mathcal{K}^\Omega \text{ s.t. } e \subset \{\partial K\}, l = l(e, K), \\ 0 & \text{otherwise,} \end{cases} \quad (\text{A.2})$$

where $(\cdot)^{-T}$ denotes the inverse-transpose matrix. In (A.2) a (piecewise-)covariant transformation has been used, as it preserves tangential traces (see [5]) on two relevant boundary segments (while allowing fully discontinuous functions on the intersections of ∂K with the skeleton $\mathcal{S}(\tilde{\mathcal{C}}^\Omega)$ of the dual complex).

For fixed polynomial order p , (A.2) is not sufficient for a complete basis: we must move back to \hat{K} and take also local shape-functions in (A.1) with $j \neq 0$. These are “bulk” basis functions, as their tangential component vanishes now on both local coordinate axes. To preserve this feature onto the global mesh, we again use their covariantly mapped versions:

$$\tilde{\mathbf{w}}_K^{ijl}(\mathbf{r}) = \begin{cases} \mathbf{A}_K^{-T} \hat{\mathbf{w}}_l^{ij}(\varphi_K^{-1}(\mathbf{r})), & \forall \mathbf{r} \in K, j > 0, \\ 0 & \text{otherwise,} \end{cases} \quad (\text{A.3})$$

where we note the appearance of K as a subscript index, rather than e , and we note that both admissible values of l now produce bulk functions. Summarizing, by grouping the $\tilde{\mathbf{w}}_e^i$ (for all i s.t. $0 \leq i \leq p$ and all $e \in \{\mathcal{S}(\mathcal{K}^\Omega) \cap \mathcal{S}(\mathcal{C}^\Omega)\}$) together with the $\tilde{\mathbf{w}}_K^{ijl}$ (for all admissible $\{i, j, l\}$ and all $K \in \mathcal{K}^\Omega$) into a new sequence $\{\tilde{\mathbf{w}}_n^p\}_{n=1}^N$, we achieve a complete set of basis functions for the space

$$\tilde{\mathbf{w}}^p := \text{Span}\{\{\tilde{\mathbf{w}}_n^p\}_{n=1}^N\} = \mathbf{H}^{\text{curl}}(\tilde{\mathcal{C}}^\Omega) \cap \mathbf{P}^p(\mathcal{K}^\Omega; \mathbb{R}^2),$$

where $\mathbf{P}^p(\mathcal{K}^\Omega; \mathbb{R}^2)$ denotes the space of vector-valued functions whose components are piecewise-polynomials of degree at most p on each $K \in \mathcal{K}^\Omega$. It is not difficult to compute the dimension of this global space for a given mesh: if we label \mathcal{E} the set of all edges in the primal complex, the n index runs from 1 to N , with

$$N = (p+1) \left(2|\mathcal{E}^\Omega| + 3p|\mathcal{C}^\Omega| \right) = 2|\mathcal{E}^\Omega| + p|\mathcal{S}(\mathcal{K}^\Omega) \cap \mathcal{S}(\mathcal{C}^\Omega)| + p(p+1)|\mathcal{K}^\Omega|, \quad (\text{A.4})$$

where the relationships between \mathcal{K}^Ω and \mathcal{C}^Ω have been used to make the splitting into lowest order, edge and bulk basis functions manifest.

For the finite-dimensional space which will be approximating the scalar $H(\mathbf{r}, t)$ instead, we proceed by first defining a new pair of oblique local coordinates $(\tilde{\xi}_1, \tilde{\xi}_2)$ on the KC element through an additional family of affine mappings $\tilde{\varphi}_K$ (and their inverses $\tilde{\varphi}_K^{-1}$), which we can construct by enforcing the origin in the associated oblique coordinates' system to coincide with the point $\tilde{O} = (1/3, 1/3)$ (for its sketch, we refer the reader again to Fig. 15), and by enforcing $0 \leq \tilde{\xi}_1, \tilde{\xi}_2 \leq 1$ on \hat{K} . Thus, by denoting the position vector with $\tilde{\mathbf{r}}$ in the new coordinates' system, we can concisely give the expressions of scalar-valued local shape-functions on \hat{K} . Namely, we introduce the monomials

$$\hat{\tilde{w}}_{\tilde{l}}^{ij}(\tilde{\mathbf{r}}) := (\tilde{\xi}_1)^i (\tilde{\xi}_{3-\tilde{l}})^j, \quad \tilde{l} \in \{1, 2\}, \quad i > 0, j \geq 0, i + j \leq p,$$

where we stress the fact that i is now a strictly positive integer. In this case, differently from the vector-valued setting, we have to consider segments $\tilde{e} \in \{\mathcal{S}(\mathcal{K}^\Omega) \cap \mathcal{S}(\tilde{\mathcal{C}}^\Omega)\}$ s.t. $\tilde{\xi}_1$ and $\tilde{\xi}_2$ provide arc-length parameters on them when moving back to any $K \in \mathcal{K}^\Omega$ in the physical mesh. Consequently we have introduced a different index $\tilde{l} = \tilde{l}(\tilde{e}, K)$. Setting $j = 0$ yields a first subset of basis functions for the global space

$$\tilde{w}_e^i(\mathbf{r}) := \begin{cases} \hat{\tilde{w}}_l^{i0}(\tilde{\varphi}_K^{-1}(\mathbf{r})) & \forall \mathbf{r} \in K \text{ s.t. } \tilde{e} \subset \partial K, \tilde{l} = \tilde{l}(\tilde{e}, K), \\ 0 & \text{otherwise,} \end{cases} \quad (\text{A.5})$$

obtained by simple piecewise combinations of local shape-functions' pull-backs. The ones in (A.5) are again edge functions (even if scalar-valued ones, their support being an edge-patch in \mathcal{K}^Ω). A new set of bulk basis functions is also present, defined by setting $\tilde{l} = 1$ (without loss of generality) and requiring $i > 0$ and $j > 0$ to hold simultaneously. The condition on i and j ensures that the associated shape-functions vanish on both $\tilde{\xi}_1 = 0$ and $\tilde{\xi}_2 = 0$ lines. Once more via pull-backs of local shape-functions onto the generic physical fundamental cell $K \in \mathcal{K}^\Omega$, we get

$$\tilde{w}_K^{ij}(\mathbf{r}) = \begin{cases} \hat{\tilde{w}}_1^{ij}(\tilde{\varphi}_K^{-1}(\mathbf{r})) & \forall \mathbf{r} \in K, i, j > 0, \\ 0 & \text{otherwise,} \end{cases} \quad (\text{A.6})$$

again using K as an index. To complete the scalar-valued basis, a third set of functions is required, namely the set

$$\tilde{w}_{\mathcal{T}} := \frac{\mathbb{1}_{\mathcal{T}}}{|\mathcal{T}|},$$

for all the triangles $\mathcal{T} \in \mathcal{C}^\Omega$, where $|\mathcal{T}|$ denotes the measure of \mathcal{T} and $\mathbb{1}_{\mathcal{T}}$ is the characteristic (or indicator) function of \mathcal{T} , i.e. the discontinuous function which takes value one for any $\mathbf{r} \in \mathcal{T}$ and zero elsewhere. Since the latter are piecewise-constant, scalar-valued functions, the mapping from reference to physical elements is trivial.

We can again group all the \tilde{w}_ℓ^i , \tilde{w}_K^{ij} and $\tilde{w}_{\mathcal{T}}$ in a new sequence of basis functions $\{\tilde{w}_m^p\}_{m=1}^M$, which provides the basis of a finite-dimensional subspace $W^p \subset H_{pw}^{curl}(\mathcal{C}^\Omega)$, where again $W^p := \text{Span}\{\tilde{w}_m^p\}_{m=1}^M$. Namely, we have constructed a basis for the vector space

$$W^p = H_{pw}^{curl}(\mathcal{C}^\Omega) \cap P^p(\mathcal{K}^\Omega; \mathbb{R}),$$

where $P^p(\mathcal{K}^\Omega; \mathbb{R})$ is the space of piecewise-polynomials of degree at most p on each $K \in \mathcal{K}^\Omega$. Once more, we can easily compute the dimension of W^p , which amounts to

$$M = \left(1 + 3p + \frac{3}{2}p(p-1)\right)|\mathcal{C}^\Omega| = |\mathcal{C}^\Omega| + p|\mathcal{S}(\tilde{\mathcal{C}}^\Omega)| + \frac{p}{2}(p-1)|\mathcal{K}^\Omega|, \quad (\text{A.7})$$

where the contributions due to the three different flavours of basis functions have been again manifestly split. We remark that basis functions can be appropriately re-ordered, by grouping members which have support contained into some common $\mathcal{T} \in \mathcal{C}^\Omega$ for the $H^{h,p}(\mathbf{r}, t)$ field, and contained into a common $\tilde{\mathcal{T}} \in \tilde{\mathcal{C}}^\Omega$ for the $\mathbf{E}^{h,p}(\mathbf{r}, t)$ field, respectively. This is not mandatory, but we thus stress the block-diagonal nature of mass-matrices $\tilde{\mathbf{M}}_p^\varepsilon$ and $\tilde{\mathbf{M}}_p^\mu$, which was achieved by breaking the standard Sobolev spaces.

Appendix B. Implementing the fully discrete scheme

Going now into greater depth with implementation-related details, we provide a procedure for the explicit computation of all matrix entries. It holds:

$$\begin{aligned} (\tilde{\mathbf{M}}_p^\varepsilon)_{n,n'} &:= \int_{\Omega} \varepsilon(\mathbf{r}) \tilde{\mathbf{w}}_{n'}^p(\mathbf{r}) \cdot \tilde{\mathbf{w}}_n^p(\mathbf{r}) \, d\mathbf{r} = \sum_{K \in \mathcal{K}^\Omega} \int_K \varepsilon(\mathbf{r}) \tilde{\mathbf{w}}_{n'}^p(\mathbf{r}) \cdot \tilde{\mathbf{w}}_n^p(\mathbf{r}) \, d\mathbf{r} = \\ &= \sum_{\substack{K \in \\ \{\mathcal{K}^\Omega \cap \text{supp}(\tilde{\mathbf{w}}_n)\}}} \int_{\hat{K}} J_K^{-1} \varepsilon(\varphi_K^{-1}(\hat{\mathbf{r}})) \mathbf{A}_K^{-T} \hat{\tilde{\mathbf{w}}}_l^{i'j'}(\hat{\mathbf{r}}) \cdot \mathbf{A}_K^{-T} \hat{\tilde{\mathbf{w}}}_l^{ij}(\hat{\mathbf{r}}) \, d\hat{\mathbf{r}} = \\ &= \sum_{\substack{K \in \\ \{\mathcal{K}^\Omega \cap \text{supp}(\tilde{\mathbf{w}}_n)\}}} \int_{\hat{K}} J_K^{-1} \mathbf{A}_K^{-1} \varepsilon(\varphi_K^{-1}(\hat{\mathbf{r}})) \mathbf{A}_K^{-T} \hat{\tilde{\mathbf{w}}}_l^{i'j'}(\hat{\mathbf{r}}), \hat{\tilde{\mathbf{w}}}_l^{ij}(\hat{\mathbf{r}}) \, d\hat{\mathbf{r}} := \\ &:= \sum_{\substack{K \in \\ \{\mathcal{K}^\Omega \cap \text{supp}(\tilde{\mathbf{w}}_n)\}}} \int_{\hat{K}} \left(\hat{\varepsilon}_K(\hat{\mathbf{r}}) \hat{\tilde{\mathbf{w}}}_l^{i'j'}(\hat{\mathbf{r}}) \right) \cdot \hat{\tilde{\mathbf{w}}}_l^{ij}(\hat{\mathbf{r}}) \, d\hat{\mathbf{r}}, \end{aligned} \quad (\text{B.1})$$

where we reach line two (in which $\text{supp}(\cdot)$ denotes the support of a function and J_K is the Jacobian determinant of φ_K) by virtue of the transformation rules in (A.2) and by using the local definition of shape-functions in (A.1). We assume that local indices i, j, l (in place of n) and i', j', l' (in place of n') exist such that the functional forms of some local shape-functions match the given $\tilde{\mathbf{w}}_{n'}^p$, $\tilde{\mathbf{w}}_n^p$. We remark that this is always true by construction of the space \tilde{W}^p . Finally, (B.1) is just a consistent re-definition where, for the sake of clarity, the modified material tensor $\hat{\varepsilon}_K := J_K^{-1} \mathbf{A}_K^{-1} \varepsilon \mathbf{A}_K^{-T}$ has been introduced.

What (B.1) means in practice is that, if the input mesh consists of straight-edged triangles and ε is piecewise-constant on each K , all inner products in the mass-matrix can be computed (off-line with respect to the rest of computation) by working on the KC element, since the Jacobian (and hence $\hat{\varepsilon}_K$) is then piecewise-constant. These conditions are very often met in practical setups. A very similar procedure applies to the mass-matrix involving the scalar unknown, where a slightly different $\hat{\mu}_K := J_K^{-1} \mu$ will arise, as the reader may also easily derive.

For the r.h.s. of (4.7), we need to compute only half of the non-zero entries, as $(\mathbf{C}_p^T)_{n,m} = (\mathbf{C}_p)_{m,n}$ (where $1 \leq n \leq N$ and $1 \leq m \leq M$). Since the involved algebra is a bit tedious, we omit in the following \mathbf{r} and $\hat{\mathbf{r}}$ dependences to make the manipulations easier to read. Furthermore we assume that we are computing an entry related to a pair of trial- and test-functions which have non-empty intersection between their support (the matrix entry is trivially null otherwise). We compute

$$\begin{aligned} (\mathbf{C}_p)_{m,n} &:= \sum_{K \in \mathcal{K}^\Omega} \int_{\partial K \cap \mathcal{S}(\mathcal{C}^\Omega)} \tilde{w}_m^p \tilde{w}_n^p \cdot \hat{\mathbf{t}}(\ell) \, d\ell + \sum_{K \in \mathcal{K}^\Omega} \int_K \tilde{w}_n^p \cdot \hat{\mathbf{z}} \times \nabla \tilde{w}_m^p \, d\mathbf{r} = \\ &= \int_{\partial K \cap \mathcal{S}(\mathcal{C}^\Omega)} \tilde{w}_m^p \tilde{w}_n^p \cdot \hat{\mathbf{t}}(\ell) \, d\ell + \int_K \tilde{w}_n^p \cdot \hat{\mathbf{z}} \times \nabla \tilde{w}_m^p \, d\mathbf{r} = \\ &= \int_{\partial \hat{K} \cap \mathcal{S}(\hat{\mathcal{T}})} J_K \hat{\tilde{w}}_l^{i'j'} \left(\mathbf{A}_K^{-T} \hat{\tilde{\mathbf{w}}}_l^{ij} \right) \cdot \left(J_K^{-1} \mathbf{A}_K \hat{\mathbf{t}}(\hat{\ell}) \right) \, d\hat{\ell} + \int_{\hat{K}} J_K \left(\mathbf{A}_K^{-T} \hat{\tilde{\mathbf{w}}}_l^{ij} \right) \cdot \left(J_K^{-1} \mathbf{A}_K \hat{\mathbf{z}} \times \hat{\nabla} \hat{\tilde{w}}_l^{i'j'} \right) \, d\hat{\mathbf{r}} = \end{aligned}$$

$$\begin{aligned}
&= \int_{\partial\hat{K} \cap \mathcal{S}(\hat{T})} \hat{\tilde{w}}_{\tilde{l}}^{i'j'} \hat{\tilde{w}}_l^{ij} \cdot \hat{\mathbf{t}}(\hat{\ell}) d\hat{\ell} + \int_{\hat{K}} \hat{\tilde{w}}_l^{ij} \cdot \hat{\mathbf{z}} \times \hat{\nabla} \hat{\tilde{w}}_{\tilde{l}}^{i'j'} d\hat{\mathbf{r}} = \\
&= \int_0^{\frac{1}{2}} \hat{\tilde{w}}_{\tilde{l}}^{i'j'} \left(\hat{\tilde{w}}_l^{ij} \cdot \hat{\xi}_1 \right) |_{\xi_2=0} d\xi_1 - \int_0^{\frac{1}{2}} \hat{\tilde{w}}_{\tilde{l}}^{i'j'} \left(\hat{\tilde{w}}_l^{ij} \cdot \hat{\xi}_2 \right) |_{\xi_1=0} d\xi_2 + \int_{\hat{K}} \hat{\tilde{w}}_l^{ij} \cdot \hat{\mathbf{z}} \times \hat{\nabla} \hat{\tilde{w}}_{\tilde{l}}^{i'j'} d\hat{\mathbf{r}}, \tag{B.2}
\end{aligned}$$

where the salient details are the following. The disappearance of summation symbols on line two descends from the fact that, for any pair of basis functions in $\mathbb{W}^p \times \tilde{\mathbb{W}}^p$, there will be at most one $K \in \mathcal{K}^\Omega$ on which neither of the two identically vanishes, which we label precisely K . Consequently, the definition of global basis functions again yields the existence of appropriate “matching” local shape-functions with respective indices $\{i, j, l\}$ and $\{i', j', \tilde{l}\}$. Line three uses the chosen transformation rules for the local shape-functions, plus the fact that the **curl** of a covariant (pseudo-)vector field, under coordinate changes, transforms according to the contra-variant (also known as Piola) mapping, which is also the appropriate transformation rule for the tangent unit vector under the same change of coordinates (proofs of this standard facts can be found, e.g., in [5]). The notation $\hat{\nabla}$ is consequently introduced for the classical differential gradient operator in the local (Cartesian) ξ_1 and ξ_2 coordinates. Line four is achieved by virtue of standard matrix-algebra simplifications. This yields the final result, in which the line- and double integrals are explicitly written in the local coordinates on \hat{K} .

The formula in (B.2) is arguably more impressive than (B.1), since no dependence on the geometry of the mesh is left after all algebraic manipulations. More in detail, all non-zero entries in the \mathbf{C}_p matrix are copies⁴ of entries of a local, entirely topological, template $\hat{M} \times \hat{N}$ matrix $\hat{\mathbf{C}}_p$, where

$$\hat{M} = \binom{p+2}{2} = \frac{(p+2)(p+1)}{2}, \quad \hat{N} = 2\hat{M},$$

are the dimensions of local scalar and vector shape-function spaces. As a consequence, with limited additional bookkeeping effort, no sparse and huge discrete curl-matrix needs to be stored in memory, and the ultra-weak curl operator can be applied efficiently, via its pre-computed low-storage representation, throughout the time integration of the problem. We remark that a similar result is achievable in more conventional DG formulations, as demonstrated in [14,46,47], yet the fact that this feat can be achieved even when using the presented novel formulation on barycentric-dual complexes was highly non-trivial.

A final important hint on implementation of the proposed discrete formulation is motivated by the fact that we found, by direct computation, the following remarkable identity to hold:

$$\int_{\hat{K}} \xi_1^r \xi_2^s d\hat{\mathbf{r}} = \frac{B_{\frac{1}{3}}(r+1, s+1)}{2^{s+1}(r+s+2)} + \frac{B_{\frac{1}{3}}(s+1, r+1)}{2^{r+1}(r+s+2)}, \tag{B.3}$$

for arbitrary non-negative integers r, s , where $B_\alpha(a, b)$ is the incomplete β -function (also known as the Euler integral of the first kind), defined as

$$B_\alpha(a, b) = \int_0^\alpha z^{a-1} (1-z)^{b-1} dz,$$

the values of which can be computed to arbitrary precision and stored for all needed positive integer values of a, b and for the particular value $\alpha = 1/3$. Since all double integrals in the discrete formulation can be shown to reduce to linear combinations of terms equivalent to the l.h.s. of (B.3), no need for numerical integration arises (as long as the material parameters are piecewise-constant).

References

- [1] K. Yee, Numerical solution of initial boundary value problems involving Maxwell's equations in isotropic media, *IEEE Trans. Antennas Propag.* 14 (1966) 302–307.
- [2] A. Taflove, S. Hagness (Eds.), *Computational Electromagnetics, the Finite Difference Time Domain Method*, 2nd ed., Artech House, 2000.
- [3] A.F. Oskooi, D. Roundy, M. Ibanescu, P. Bermel, J. Joannopoulos, S.G. Johnson, Meep: a flexible free-software package for electromagnetic simulations by the FDTD method, *Comput. Phys. Commun.* 181 (2010) 687–702.
- [4] J. Jin, *The Finite Element Method in Electromagnetics*, 3rd ed., Wiley-IEEE Press, 2014.
- [5] P. Monk, *Numerical Methods for Maxwell's Equations*, Numerical Mathematics and Scientific Computation, Clarendon Press, 2003.
- [6] J.C. Nedelec, Mixed finite elements in \mathbb{R}^3 , *Numer. Math.* 35 (1980) 315–341.
- [7] D.A. White, Orthogonal vector basis functions for time domain finite element solution of the vector wave equation [EM field analysis], *IEEE Trans. Magn.* 35 (1999) 1458–1461.

⁴ up to orientation of edges and triangles, from which a very small number of equivalence classes for $\hat{\mathbf{C}}_p$ can be derived.

- [8] A. Elmquist, P. Joly, Éléments finis d'arête et condensation de masse pour les équations de Maxwell: le cas 2D, *C. R. Acad. Sci., Ser. 1 Math.* 324 (1997) 1287–1293.
- [9] G. Cohen, P. Monk, Gauss point mass lumping schemes for Maxwell's equations, *Numer. Methods Partial Differ. Equ.* 14 (1998) 63–88.
- [10] H. Egger, B. Radu, A mass-lumped mixed finite element method for Maxwell's equations, in: G. Nicosia, V. Romano (Eds.), *Scientific Computing in Electrical Engineering*, Springer International Publishing, Cham, 2020, pp. 15–24.
- [11] A. Bossavit, Solving Maxwell equations in a closed cavity, and the question of 'spurious modes', *IEEE Trans. Magn.* 26 (1990) 702–705.
- [12] J. Hesthaven, T. Warburton, Nodal high-order methods on unstructured grids: I. Time-domain solution of Maxwell's equations, *J. Comput. Phys.* 181 (2002) 186–221.
- [13] M.J. Grote, T. Mitkova, Explicit local time-stepping methods for Maxwell's equations, *J. Comput. Appl. Math.* 234 (2010) 3283–3302.
- [14] C. Koutschan, C. Lehrenfeld, J. Schöberl, *Computer Algebra Meets Finite Elements: An Efficient Implementation for Maxwell's Equations*, Springer Vienna, Vienna, 2012, pp. 105–121.
- [15] Y. Huang, J. Li, W. Yang, Interior penalty DG methods for Maxwell's equations in dispersive media, *J. Comput. Phys.* 230 (2011) 4559–4570.
- [16] T. Weiland, Time domain electromagnetic field computation with finite difference methods, *Int. J. Numer. Model.* 9 (1996) 295–319.
- [17] T. Matsuo, Space-time finite integration method for electromagnetic field computation, *IEEE Trans. Magn.* 47 (2011) 1530–1533.
- [18] E.T. Chung, P. Ciarlet, T.F. Yu, Convergence and superconvergence of staggered discontinuous Galerkin methods for the three-dimensional Maxwell's equations on Cartesian grids, *J. Comput. Phys.* 235 (2013) 14–31.
- [19] E. Tonti, Finite formulation of the electromagnetic field, *Prog. Electromagn. Res.* 32 (2001) 1–44.
- [20] M. Marrone, Computational aspects of the cell method in electrodynamics, *Prog. Electromagn. Res. (PIER)* 32 (2001) 317–356.
- [21] L. Codicosa, M. Politi, Explicit, consistent, and conditionally stable extension of FD-TD to tetrahedral grids by fit, *IEEE Trans. Magn.* 44 (2008) 1258–1261.
- [22] P. Alotto, A. De Cian, G. Molinari, A time-domain 3-d full-Maxwell solver based on the cell method, *IEEE Trans. Magn.* 42 (2006) 799–802.
- [23] L. Codicosa, B. Kapidani, R. Specogna, F. Trevisan, Novel FDTD technique over tetrahedral grids for conductive media, *IEEE Trans. Antennas Propag.* 66 (2018) 5387–5396.
- [24] A. Stern, Y. Tong, M. Desbrun, J.E. Marsden, *Geometric Computational Electrodynamics with Variational Integrators and Discrete Differential Forms*, Springer New York, New York, NY, 2015, pp. 437–475.
- [25] F.L. Teixeira, W.C. Chew, Lattice electromagnetic theory from a topological viewpoint, *J. Math. Phys.* 40 (1999) 169–187.
- [26] R. Hiptmair, Discrete Hodge operators, *Numer. Math.* 90 (2001) 265–289.
- [27] T. Tarhasaari, L. Kettunen, A. Bossavit, Some realizations of a discrete Hodge operator: a reinterpretation of finite element techniques [for EM field analysis], *IEEE Trans. Magn.* 35 (1999) 1494–1497.
- [28] A. Bossavit, L. Kettunen, Yee-like schemes on staggered cellular grids: a synthesis between fit and fem approaches, *IEEE Trans. Magn.* 36 (2000) 861–867.
- [29] B. Auchmann, S. Kurz, A geometrically defined discrete Hodge operator on simplicial cells, *IEEE Trans. Magn.* 42 (2006) 643–646.
- [30] D.A. Di Pietro, B. Kapidani, R. Specogna, F. Trevisan, An arbitrary-order discontinuous skeletal method for solving electrostatics on general polyhedral meshes, *IEEE Trans. Magn.* 53 (2017) 1–4.
- [31] B. Kapidani, L. Codicosa, R. Specogna, The time-domain cell method is a coupling of two explicit discontinuous Galerkin schemes with continuous fluxes, *IEEE Trans. Magn.* 56 (2020) 1–4.
- [32] J. Schöberl, Netgen an advancing front 2D/3D-mesh generator based on abstract rules, *Comput. Vis. Sci.* 1 (1997) 41–52.
- [33] P.-O. Persson, G. Strang, A simple mesh generator in MATLAB, *SIAM Rev.* 46 (2004) 329–345.
- [34] R.J. LeVeque, *Finite Volume Methods for Hyperbolic Problems*, Cambridge Texts in Applied Mathematics, Cambridge University Press, 2002.
- [35] H. Egger, F. Kretzschmar, S.M. Schnepf, T. Weiland, A space-time discontinuous Galerkin Trefftz method for time dependent Maxwell's equations, *SIAM J. Sci. Comput.* 37 (2015) B689–B711.
- [36] E. Forest, R.D. Ruth, Fourth-order symplectic integration, *Phys. D Nonlin. Phenom.* 43 (1990) 105–117.
- [37] V.A. Titarev, E.F. Toro, Ader: arbitrary high order Godunov approach, *J. Sci. Comput.* 17 (2002) 609–618.
- [38] Y. Sun, P. Tse, Symplectic and multisymplectic numerical methods for Maxwell's equations, *J. Comput. Phys.* 230 (2011) 2076–2094.
- [39] M. Cicuttin, L. Codicosa, B. Kapidani, R. Specogna, F. Trevisan, Gpu accelerated time-domain discrete geometric approach method for Maxwell's equations on tetrahedral grids, *IEEE Trans. Magn.* 54 (2018) 1–4.
- [40] G.W. Stewart, A Krylov–Schur algorithm for large eigenproblems, *SIAM J. Matrix Anal. Appl.* 23 (2002) 601–614.
- [41] A. Buffa, I. Perugia, Discontinuous Galerkin approximation of the Maxwell eigenproblem, *SIAM J. Numer. Anal.* 44 (2006) 2198–2226.
- [42] J. Hesthaven, T. Warburton, *Nodal Discontinuous Galerkin Methods: I. Algorithms, Analysis, and Applications*, Springer, 2008.
- [43] L. Pincherle, Electromagnetic waves in metal tubes filled longitudinally with two dielectrics, *Phys. Rev.* 66 (1944).
- [44] M. Dauge, Personal website, <https://perso.univ-rennes1.fr/monique.dauge/benchmax.html>, 2004. (Accessed October 2019).
- [45] I. Babuška, M. Griebel, J. Pitkäranta, The problem of selecting the shape functions for a p-type finite element, *Int. J. Numer. Methods Eng.* 28 (1989) 1891–1908.
- [46] T. Warburton, A low-storage curvilinear discontinuous Galerkin method for wave problems, *SIAM J. Sci. Comput.* 35 (2013) A1987–A2012.
- [47] B. Kapidani, J. Schöberl, A matrix-free discontinuous Galerkin method for the time dependent Maxwell equations in unbounded domains, preprint, <https://arxiv.org/abs/2002.08733>, 2020.